

The Role of Type Ia Supernovae in Chemical Evolution I: Lifetime of Type Ia Supernovae and Galactic Supernova Rates

Chiaki KOBAYASHI¹ and Ken'ichi NOMOTO^{2,3}

¹ *Division of Theoretical Astronomy, National Astronomical Observatory of Japan,
Mitaka-shi, Tokyo 181-8588, Japan; chiaki@th.nao.ac.jp*

² *Department of Astronomy, School of Science, University of Tokyo, Bunkyo-ku, Tokyo
113-0033, Japan; nomoto@astron.s.u-tokyo.ac.jp*

³ *Institute for the Physics and Mathematics of the Universe, University of Tokyo, Kashiwa,
Chiba 277-8582, Japan*

ABSTRACT

We construct a new model of Type Ia Supernovae (SNe Ia), based on the single degenerate scenario, taking account of the metallicity effect of the white dwarf (WD) wind and the mass-stripping effect on the binary companion star. Our model naturally predicts that the SN Ia lifetime distribution spans a range of 0.1 – 20 Gyr with the double peaks at ~ 0.1 and 1 Gyr. While the present SN Ia rate in elliptical galaxies can be reproduced with the old population of the red-giants+WD systems, the large SN Ia rate in radio galaxies could be explained with the young population of the main-sequence+WD systems. Because of the metallicity effect, i.e., because of the lack of winds from WDs in the binary systems, the SN Ia rate in the systems with $[\text{Fe}/\text{H}] \lesssim -1$, e.g., high- z spiral galaxies, is supposed to be very small. Our SN Ia model can give better reproduction of the $[(\alpha, \text{Mn}, \text{Zn})/\text{Fe}]-[\text{Fe}/\text{H}]$ relations in the solar neighborhood than other models such as the double-degenerate scenario. The presence of the young population of SNe Ia strongly favors the presence of the metallicity effect. We also succeed in reproducing the galactic supernova rates with their dependence on the morphological type of galaxies, and the cosmic SN Ia rate history with a peak at $z \sim 1$. At $z \gtrsim 1$, the predicted SN Ia rate decreases toward higher redshifts and SNe Ia will be observed only in the systems that have evolved with a short timescale of chemical enrichment. This suggests that the evolution effect in the supernova cosmology can be small.

Subject headings: galaxies: abundances — galaxies: evolution — stars: supernovae

1. Introduction

The star formation histories of galaxies are imprinted on stellar populations of the galaxies. Because of the age-metallicity degeneracy for stellar populations, it is difficult to determine “age” from their colors and spectra alone. However, the elemental abundance ratios can provide independent information on “age”, because different heavy elements are produced from different supernovae with different timescales (e.g., Pagel 1997; Matteucci 2001). To derive the information of “ages” from elemental abundance patterns as a cosmic clock, the most important uncertainty is the lifetime of Type Ia Supernovae (SNe Ia), i.e., the evolutionary time (delay-time) of the progenitor from the main-sequence through the explosion, which is mainly determined by the lifetime of the relatively low-mass ($\lesssim 8M_{\odot}$) companion star of the exploding white dwarf (WD).

There exist two distinct types of supernova explosions (e.g., Arnett 1996; Filippenko 1997): One is Type II supernovae (SNe II), which are the core collapse-induced explosions of massive stars ($\gtrsim 8M_{\odot}$) with short lifetimes of 10^{6-7} yrs, and produce more α -elements (O, Mg, Si, S, Ca, and Ti) relative to Fe with respect to the solar ratios (i.e., $[\alpha/\text{Fe}] > 0$). Type Ib and Ic Supernovae (SNe Ib and Ic) are also the core-collapse supernovae, but have lost the envelope material before the explosions. Recently, it is found that bright core-collapse supernovae, hypernovae (HNe), produce an important amount of Fe (e.g., Nomoto et al. 2006). In chemical evolution models, the contributions of SNe Ib, Ic, and HNe can be included in that of SNe II (Kobayashi et al. 2006). The other is SNe Ia, which are the thermonuclear explosions of accreting WDs in close binaries and produce mostly Fe and little α -elements (e.g., Nomoto et al. 1994; Hillebrandt & Niemeyer 2000). The progenitors of the majority of SNe Ia are most likely the Chandrasekhar (Ch) mass WDs (e.g., Nomoto, Iwamoto & Kishimoto 1997 for a review; see also Nomoto et al. 2007), although the sub-Ch mass models might correspond to some peculiar subluminous SNe Ia. The early time spectra of the majority of SNe Ia are in excellent agreement with the synthetic spectra of the Ch mass models, while the spectra of the sub-Ch mass models are too blue to be compatible with observations (Höfllich & Khokhlov 1996; Nugent et al. 1997).

For the evolution of accreting C+O WDs toward the Ch mass, two scenarios have been proposed: One is a double-degenerate (DD) scenario, i.e., merging of double C+O WDs with a combined mass surpassing the Ch mass limit takes place (Iben & Tutukov 1984; Webbink 1984), and the other is a single-degenerate (SD) scenario, i.e., the WD mass grows by accretion of hydrogen-rich matter via mass transfer from a binary companion (e.g., Nomoto et al. 2000; Livio 2001, for reviews). From the long-term observational search (SPY project) of the WD binaries for the DD systems, more than thousand WDs are found (Napiwotzki 2007; Geier et al. 2007). However, their combined masses are smaller than the

Ch mass, except for the one candidate near the Ch mass, although its secondary star has not been detected (Napiwotzki et al. 2005). Theoretically, it has been suggested that the merging of WDs leads to accretion-induced collapse rather than SNe Ia (Saio & Nomoto 1985, 1998).

The lifetime of SNe Ia have been estimated from different aspects as follows, and these estimates conflict each other: (1) *Population synthesis* — The lifetime distribution of SNe Ia has been predicted with the population synthesis models for the evolution of binary systems (e.g., Yungelson 2005). The predicted rate of SD systems in those models is much smaller than DD systems, and the majority of SNe Ia have the lifetime as short as ~ 0.1 Gyr (e.g., Yungelson & Livio 1998; Canal, Méndez, & Ruiz-Lapuente 2001). However, the optically thick winds from the WD, which were not taken into account in the above models, have been shown to play an essential role in the evolution of the accreting WDs (Hachisu, Kato & Nomoto 1996, 1999a; Hachisu et al. 1999b). Furthermore, the stripping effect may increase the parameter space for the SD systems (Hachisu, Kato & Nomoto 2007). If these effects are taken into account in the population synthesis models, the DD rate could be smaller, and the SD rate could be larger.

(2) *Chemical evolution* — The typical lifetime of SNe Ia could have been constrained from the chemical evolution of the Milky Way Galaxy, most notably in the $[\alpha/\text{Fe}]$ - $[\text{Fe}/\text{H}]$ relations. Metal-poor stars with $[\text{Fe}/\text{H}] \lesssim -1$ have $[\alpha/\text{Fe}] \sim 0.5$ for Mg, Si, and Ca on the average (e.g., McWilliam et al. 1995; Cayrel et al. 2004), while disk stars with $[\text{Fe}/\text{H}] \gtrsim -1$ show a decrease in $[\alpha/\text{Fe}]$ with increasing metallicity (e.g., Edvardsson et al. 1993; Bensby et al. 2004). Such an evolutionary change in $[\alpha/\text{Fe}]$ against $[\text{Fe}/\text{H}]$ has been explained with the early heavy-element production by SNe II and the delayed enrichment of Fe by SNe Ia (Matteucci & Greggio 1986). Conversely, chemical evolution models can constrain the nature of progenitor systems of SNe Ia; for example, Yoshii, Tsujimoto, & Nomoto (1996) estimated the lifetime of SN Ia progenitors to be as long as $0.5 - 3$ Gyr.

(3) *Supernova rates* — The redshift evolution of the SN Ia rate can give a rough estimate of the typical lifetime of SNe Ia (i.e., delay-time) for the assumed star formation history. The decrease of the SN Ia rate seen at $z \sim 1$ corresponds to the delay-time of ~ 3 Gyr (Strolger et al. 2004). However, the observed cosmic star formation rates (SFRs) involve uncertainties from dust extinction and completeness. The environmental dependence on galaxy evolution must be important if the SNe Ia rate depends on metallicity. SN Ia rates depending on the galaxy type can give stronger constraint on the SN Ia progenitor models. Della Valle et al. (2005) suggested that the short lifetime of ~ 0.1 Gyr is required to explain the high SN Ia rate in radio-loud elliptical galaxies, and Sullivan et al. (2006) suggested the similar lifetime distribution from the relation between the SN Ia rate and the specific SFR.

Therefore, the bimodal distribution of the lifetime of SNe Ia, so-called “A+B” model, has been proposed (Scannapieco & Bildsten 2005; Mannucci et al. 2006).

In addition, Kobayashi et al. (1998, hereafter K98) have found the metallicity effect on the WD winds, consequently, on the occurrence of SNe Ia, based on the simulations of the progenitor evolution by Hachisu et al. (1999ab). If the iron abundance of the progenitors is as low as $[\text{Fe}/\text{H}] \lesssim -1.1$, then the wind is too weak for SNe Ia to occur. Thus the SN Ia rate in the system with $[\text{Fe}/\text{H}] \lesssim -1.1$ is supposed to be very small. Several SNe Ia have been observed in dwarf galaxies, but the metallicity of these galaxies are larger than $[\text{Fe}/\text{H}] \sim -1$ (Kobayashi, Tsujimoto, & Nomoto 2000, hereafter K00; Hamuy et al. 2001). The existence of the secondary parameter, the metallicity of SN Ia progenitors, means that there is “the time-metallicity degeneracy” also for the abundance ratios. The estimates of the age of universe and star formation histories of galaxies from their abundance ratios should be taken care. The redshift evolution of the cosmic SN Ia rate is also affected by this metallicity effect.

The modeling of SNe Ia in the chemical evolution was first made by Greggio & Renzini (1983), where the SN Ia rate is calculated from the distribution of binaries based on Whelan & Iben (1973). The upper and lower mass limits are set to describe the DD scenario (Greggio & Renzini 1983), and then extended for the SD scenario (Greggio 1996). This model has recently been updated in Greggio (2005) and Matteucci et al. (2006). An alternative model was proposed by K98, fully based on the SD scenario, where the metallicity effect is essential to explain the $[\text{O}/\text{Fe}]$ - $[\text{Fe}/\text{H}]$ relation in the solar neighborhood. K00 applied this model for different types of galaxies, and succeeded in reproducing the present SN II and Ia rates in different types of galaxies. Matteucci & Recchi (2001, hereafter MR01), however, argued that they could not reproduce K98 results and that the lack of SNe Ia at low metallicities produces results at variance with the observed $[\text{O}/\text{Fe}]$ - $[\text{Fe}/\text{H}]$ relation. However, this is due to their misunderstanding of the parametrization of the K98 models, as described in detail in §5.

In this paper, we first show the lifetime distribution functions derived from different SN Ia models. We then introduce our new SN Ia model by taking into account the stripping effect (Hachisu, Kato & Nomoto 2007) and show the lifetime distribution function as a function of metallicity (§2). We then evaluate the SN Ia models from the comparison with observations. The evolution of the elemental abundance ratios in the solar neighborhood (§3) and the galactic and cosmic supernova rates (§4) can be better reproduced with our SN Ia model including the metallicity effect. In §5, we discuss the two formulations in K98 and MR01 in detail, and reproduce both results using the alternative formulation. In §6, we summarize our conclusions. The discussion on the elemental abundance ratios in other galaxies will be

included in the second paper.

2. Lifetime Distribution

2.1. Previous Models of Type Ia Supernovae

Lifetime (i.e., delay-time) of SNe Ia is not a single parameter. The SN Ia lifetime, t_{Ia} , can be determined from the lifetime of companion stars in C+O WD binary systems, because the time interval from the start of mass accretion to the explosion is as short as $\lesssim 10^7$ yr. Since the companion’s mass ranges are different among various SN Ia scenarios, the typical lifetime is different for the different SN Ia models. In the chemical evolution models, two formulations have been proposed in K00 and MR01 (see §5 for details). For the DD scenario, the timescale of gravitational radiation until the two WDs start to merge is also important, and the lifetime distribution functions have been provided from the population synthesis of the binary evolution. We adopt the Tutukov & Yungelson (1994)’s function into our chemical evolution model for the DD model.

Figure 1 shows the distribution functions of the companion’s mass (upper panel) and lifetime (lower panel) for the three SN Ia models. These correspond to the SN Ia rate of the simple stellar population, which is defined as a single generation of stars with the same age and metallicity.

- The red solid and short-dashed lines show the distributions for the K98 model, which are the same as in K00, but multiplied by the number fraction of WDs, $\int \frac{1}{m_1} \phi(m_1) dm_1 = 0.019$. The resultant lifetime distribution slightly depends on metallicity (solid lines, $Z = 0.002$; short-dashed lines, $Z = 0.02$). The two components appear at $(m_d, t_{\text{Ia}}) = (\sim 2M_\odot, 0.5 - 1.5 \text{ Gyr})$ and $(\sim 1M_\odot, 2 - 20 \text{ Gyr})$, which correspond to the two types of binary systems, the MS+WD and RG+WD systems, respectively. The bi-modality, which is observationally proposed as the “A+B” model, have been naturally realised in our model.
- The green dot-dashed line shows the lifetime distribution for the DD scenario. The corresponding mass distributions span a range of $1 - 5M_\odot$. Because $\frac{dm_d}{dt_{\text{Ia}}}$ is larger for larger m_d , a typical lifetime is $t_{\text{Ia}} \sim 0.1 \text{ Gyr}$, the fraction with $\gtrsim 1 \text{ Gyr}$ is very small, and the fraction with $\gtrsim 10 \text{ Gyr}$ is almost zero.
- The blue long-dashed lines is for the MR01 model, although the initial mass function (IMF) and the mass-lifetime relation is the same as our models (§5). The mass distribution extends over $0 - 8M_\odot$ having a peak at $\sim 1.5M_\odot$. The decrease of the rate

toward larger m_2 is due to the IMF, and the decrease toward smaller m_2 is caused by $m_1 + m_2 \geq 3M_\odot$. A typical lifetime is $t_{\text{Ia}} \sim 0.3$ Gyr, which is longer than the DD model. The fraction with $\gtrsim 1$ Gyr is two times larger than the DD model, and the fraction with $\gtrsim 10$ Gyr is small but not zero.

For each SN Ia progenitor model, the distribution function of the companion’s mass and lifetime, i.e., the SN Ia rate in $1M_\odot$ of simple stellar population is given in Tables 1-3.

2.2. A New SN Ia Model

Hachisu et al. (2007, hereafter HKN07) introduced the stripping effect, where a part of the envelope mass of the companion stars is stripped by the interaction with the WD winds. The efficiency is described by one parameter c , which depends mainly on the wind velocity. The effect of geometry can be given as a function of the mass ratio, and is included in c . The value of c can be determined from the observed binary systems such as supersoft X-ray sources.

Although the wind velocity depends on the metallicity, the binary evolution is calculated only for $Z = 0.02$ in HKN07. We thus adopt the results for $Z = 0.02$ with $c = 3$, and apply to other metallicities by taking account of the metallicity dependence of the WD winds (Hachisu 2007, private communication). In the present model, the metallicity effect is included in the parameter space of the binary systems that leads to SNe Ia, in contrast to the simple cut-off the SN Ia rate in K98 and K00. The formulation is the same as Eq.[2] (see §5), but the upper and lower mass of the binary systems, m_u and m_ℓ , depend on $[\text{Fe}/\text{H}]$, as summarised in Table 4. For the opacity of the WD winds, iron is the most effective element. Figure 2 shows the SN Ia rate in the simple stellar population as functions of companion’s mass (upper panel)

Table 4. Upper and lower mass of the binary companion of SN Ia progenitor systems depending on the iron abundance, in the mass unit of M_\odot .

$[\text{Fe}/\text{H}]$	-1.1	-1.0	-0.7	0	0.4
$m_{\text{RG},\ell}$	0.9	0.9	0.9	0.9	0.8
$m_{\text{RG},u}$	0.9	1.5	2.0	3.0	3.5
$m_{\text{MS},\ell}$	1.8	1.8	1.8	1.8	1.8
$m_{\text{MS},u}$	1.8	2.6	4.0	5.5	6.0

and lifetime (lower panel) for the metallicity $Z = 0.002$ (blue), 0.004 (green), 0.02 (orange), and 0.05 (red). The solid and dashed lines indicate the MS+WD and RG+WD systems that correspond to the young and old population of SNe Ia, respectively. Note that the absolute numbers, i.e., b parameters, are determined to reproduce the chemical evolution in the solar neighborhood.

Figure 3 shows the summation of the young and old components of the SN Ia rate as functions of companion’s mass (upper panel) and lifetime (lower panel). The bimodal distribution is realised at $(m_d, t_{\text{Ia}}) = (\sim 2M_\odot, 0.1 - 0.5 \text{ Gyr})$ and $(\sim 1M_\odot, 1 - 3 \text{ Gyr})$ corresponding to the MS+WD and RG+WD systems, respectively. The two peaks are seen at $t_{\text{Ia}} \sim 0.5$ and 3 Gyr for $Z = 0.002$ (blue short-dashed line), at $t_{\text{Ia}} \sim 0.2$ and 1 Gyr for $Z = 0.004$ (green solid lines), at $t_{\text{Ia}} \sim 0.1$ and 1 Gyr for $Z = 0.02$ (orange dotted line) and 0.05 (red long-dashed line). For higher metallicity, the lifetime distribution extends to both shorter and longer lifetimes. Such a short lifetime as $t_{\text{Ia}} \sim 0.1$ Gyr is caused by the stripping effect that enables the accreting WDs with massive ($\sim 6 - 8M_\odot$) companions to explode. The lifetime as long as $t_{\text{Ia}} \sim 20$ Gyr is caused by the elongation of the lifetime of small-mass companion stars, which is dominant in present-day elliptical galaxies.

3. [X/Fe]-[Fe/H] Relations

Using the one-zone chemical evolution model, we show the evolution of elemental abundance ratios in the solar neighborhood for different SN Ia models. The star formation history is determined from the following observations in the solar neighborhood. The formulations of the infall rate and the SFR are the same as K98 and K06 (see also Figure 6 in K06). The input parameters are the Galactic age of 13 Gyr and accretion timescale $\tau_i = 5$ Gyr. The star formation timescale $\tau_s = 2.2$ Gyr is determined from the present gas fraction $f_g = 0.15$ (see K00 for the definition). The same parameters are set for the other SN Ia models, because the contribution of SNe Ia on the gas fraction is negligible.

Figure 4 shows (a) the SFR, (b) the age-metallicity relations, and (c) the metallicity distribution function (MDF) for different SN Ia models. The resultant SFR peaks at $t \sim 8$ Gyr, but does not very much change for $t \sim 5 - 13$ Gyrs, and the present SFR is consistent with the observational estimate. The red solid, cyan dotted, green short-dashed, blue long-dashed, and magenta dot-dashed lines are for our new model with and without the metallicity effect, the DD, MR01, and K98 models, respectively. All models can give excellent agreement with these observations. Compared with the K98 model (magenta dot-dashed line), our new SN Ia model (red solid line) gives slightly slower increase in $[\text{Fe}/\text{H}]$ after $[\text{Fe}/\text{H}] \sim -1$ (panel b), and slightly larger number of metal-poor stars around $[\text{Fe}/\text{H}] \sim -1$ (panel c). This

is because the metallicity effect is included not with a sharp cut-off but with a gradual decrease in our new model. Recently, Nordström et al. (2004) showed a narrower MDF than the plotted observations (Edvardsson et al. 1993; Wyse & Gilmore 1995), which may suggest that a sharp cut-off exist in the SN Ia rate at $[\text{Fe}/\text{H}] \sim -1$.

For the MR01 and DD models, the parameter A for the total number of SNe Ia is chosen to meet the MDF. For the MR01 model, the binary fraction of $A = 0.035$ adopted above is better than 0.05 in MR01. For the DD model, the total fraction of SNe Ia is set to be 0.001. In our models, the combination of the b parameters can be determined from the metal-rich end of the MDF. We choose $[b_{\text{RG}}, b_{\text{MS}}]=[0.23, 0.23]$, although the models with $[0.15, 0.28]$, $[0.10, 0.32]$ and $[0.05, 0.35]$ are also possible. For the case without metallicity effect (the companion’s mass range for $Z = 0.02$ is adopted), $[b_{\text{RG}}, b_{\text{MS}}]=[0.27, 0.27]$. For K98’s SN Ia model, $[b_{\text{RG}}, b_{\text{MS}}]=[0.02, 0.04]$, which are smaller than K98 $[0.04, 0.04]$ and K00 $[0.02, 0.05]$ because nucleosynthesis yields are updated (K06).

In the solar neighborhood, elemental abundance ratios are observed for a number of stars over a wide range of metallicity, which gives one of the most stringent constraints on the progenitors of SNe Ia. Figures 5 and 6 show the evolutions of elemental abundance ratios $[\text{X}/\text{Fe}]$ for O, Mg, Mn, and Zn, against the iron abundance $[\text{Fe}/\text{H}]$.

In the early stage of the galaxy formation, only SNe II explode, and $[\alpha/\text{Fe}]$ stays constant. Because of the delayed Fe production by SNe Ia, $[\alpha/\text{Fe}]$ decreases toward 0. Although some observations with UV OH lines, which are not plotted here, show a monotonic increase in $[\text{O}/\text{H}]$ towards lower metallicity (Israeli et al. 1998; Boesgaard et al. 1999), the O observations with the forbidden line and infrared lines and the observations for the other α -elements (Mg, Si, Ca, and Ti) show the plateau rather than the increase.

Manganese shows a characteristic behavior. Since SNe Ia produce $[\text{Mn}/\text{Fe}] > 0$, $[\text{Mn}/\text{Fe}]$ increases toward higher metallicity (K06). This evolutionary change is started from the same $[\text{Fe}/\text{H}]$ as the decreasing trends of $[\alpha/\text{Fe}]$. Note that Mn yield may depend on the metallicity in the nucleosynthesis of SNe Ia.

The species of zinc depend on the metallicity. At low metallicity, ^{64}Zn is produced by complete Si-burning in HNe (Umeda & Nomoto 2002), which are assumed to be a half of massive ($\geq 20M_{\odot}$) SNe II with the lifetime of $\lesssim 10^7$ yr (K06). At high metallicity, neutron-rich isotopes of zinc, $^{66-70}\text{Zn}$ are produced by neutron-capture in He and C burning, which is larger for higher metallicity (Fig. 5 in K06) and ejected by SNe II. Because of the combination of the lifetime and metallicity effects, $[\text{Zn}/\text{Fe}]$ shows an interesting track. The lifetime distribution is different for the different models of SNe Ia, and the metallicity effect is additionally included in our SN Ia models.

- In the DD model (green short-dashed line), $[\alpha/\text{Fe}]$ decreases and $[\text{Mn}/\text{Fe}]$ increases too early and too quickly from $[\text{Fe}/\text{H}] \sim -2$ compared with the observations. This is because the lifetime of the majority of SNe Ia is shorter than 0.3 Gyr (Fig. 1). The SN Ia lifetime is so short that $[\text{Zn}/\text{Fe}]$ decreases by 0.25 dex from $[\text{Fe}/\text{H}] \sim -2$ to ~ -0.6 . Because the SN Ia rate sharply decreases for longer lifetime, and because the SFR does not change very much, the contribution of HNe becomes larger than SNe Ia at later time. This results in the increase from $[\text{Fe}/\text{H}] \sim -0.6$ to ~ 0 , which is not seen in the observations.
- In the MR01 model reproduced with our code (blue long-dashed line), the decrease in $[\alpha/\text{Fe}]$ and the increase in $[\text{Mn}/\text{Fe}]$ are seen at $[\text{Fe}/\text{H}] \sim -2$ as early as in the DD model. The slope of $[\alpha/\text{Fe}]$ and $[\text{Mn}/\text{Fe}]$ against $[\text{Fe}/\text{H}]$ is a little shallower than the DD model because the fraction of lifetime with $\gtrsim 1$ Gyr is larger. The $[\text{Zn}/\text{Fe}]$ decreases only by 0.15 dex from $[\text{Fe}/\text{H}] \sim -2$ to ~ -0.6 .
- Our SN Ia model with the metallicity effect (red solid line) gives the best agreement with the observations. The decrease in $[\alpha/\text{Fe}]$ and the increase in $[\text{Mn}/\text{Fe}]$ are determined not from the lifetime effect but from the metallicity effect on the SN Ia rate. Since the lowest metallicity to produce SNe Ia is $[\text{Fe}/\text{H}] = -1.1$, the evolutionary change is caused at $[\text{Fe}/\text{H}] \sim -1$ by the companion stars with $M_{\text{MS},u} = 2.6M_{\odot}$ after the main-sequence lifetime of ~ 0.5 Gyr. In the K98 model, the metallicity effect is included more sharply, and thus the evolutionary change appears a bit more sharply. Different from the DD and MR01 models, $[\text{Zn}/\text{Fe}]$ increases from $[\text{Fe}/\text{H}] \sim -1.5$ by the metallicity effect on Zn yield, and decreases from $[\text{Fe}/\text{H}] \sim -1$ by the contribution of SNe Ia. This trend seems to be consistent with observations. Further observations of these elements at $[\text{Fe}/\text{H}] \gtrsim -1.5$ is critically important in order to identify the SN Ia progenitors and to clarify the metallicity dependence on the nucleosynthesis yields.
- If we do not include the metallicity effect (dotted line in Fig. 6), $[\alpha/\text{Fe}]$ starts to decrease at $[\text{Fe}/\text{H}] \sim -2$. This corresponds to the shortest SN Ia lifetime of ~ 0.1 Gyr for $M_{\text{MS},u} = 5.5M_{\odot}$. This is too early to be compatible with the observations. Such a too early decrease in $[\alpha/\text{Fe}]$ starts at $[\text{Fe}/\text{H}] \sim -1.5$ in the K98 model (see Fig. 3 in K98), because the shortest lifetime (~ 0.5 Gyr for $M_{\text{MS},u} = 2.6M_{\odot}$) is longer. In our new model without the metallicity effect, this inconsistency is more serious than in K98, because the younger population of SNe Ia causes the decrease in $[\alpha/\text{Fe}]$ at much smaller $[\text{Fe}/\text{H}]$.

Mannucci et al. (2006) suggested that 35 – 50% of SNe Ia should be composed by the systems with lifetimes as short as 0.1 Gyr. On the other hand, Matteucci et al. (2006)

claimed that the fraction should be less than $\sim 35\%$ in order to explain the [O/Fe]-[Fe/H] relation and iron abundance in the intracluster medium. In our model, 50% of SNe Ia come from the MS+WD systems. If the fraction of the young population of SNe Ia is so large, the metallicity effect is strongly required from the chemical evolution of the solar neighborhood.

4. Galactic Supernovae Rate

4.1. SN Ia rate in Ellipticals

The present SN Ia rate in elliptical galaxies gives also a stringent constraint on the SN Ia progenitor models. Figure 7 shows the SN Ia rate history in ellipticals, which is similar to Figure 5 of K00, but for the cosmological parameters of $H_0 = 70 \text{ km s}^{-1} \text{ Mpc}^{-1}$, $\Omega_0 = 0.3$, $\lambda_0 = 0.7$, and the galactic age of 13 Gyr. (Note that the observed SN Ia rate is proportional to H_0^2 .) The star formation history is assumed as in K00; the bulk of stars in ellipticals are formed at $z \gtrsim 3$, and thus having ages older than 10 Gyr (see Table 5). The present B-V color of 0.9 (Roberts & Haynes 1994) and the mean stellar metallicity of ~ -0.5 (Kobayashi & Arimoto 1999) are reproduced. The present stellar mass-to-light ratio is $M/L_K = 1.8$ and $M/L_B = 9.2$ in our model. The resultant SFR is similar to the SN II rate (black dot-dashed line).

- In the DD model (green short-dashed line), the SN Ia lifetimes are too short to explain the observed SN Ia rate at the present epoch (Cappellaro et al. 1999). Toward $z \sim 4$, the SN Ia rate rapidly increases, and the SN Ia rate at $z \sim 4$ is 10 times larger than the present rate.

Table 5. The input parameters of galaxy models; timescales of the star formation and inflow in Gyr.

	τ_s [Gyr]	τ_i [Gyr]
E	0.1	0.1
S0a/Sa	1.8	2.0
Sab/Sb	1.75	4.5
Sbc/Sc	2.0	8.3
Scd/Sd	2.1	23.0

- In the MR01 model (blue long-dashed line), the fraction of SNe Ia with $t_{\text{Ia}} \gtrsim 10$ Gyr is larger than the DD model, so that the present rate is not too small compared with the observation. Toward $z \sim 3$, the SN Ia rate gradually increases, and the SN Ia rate at $z \sim 1$ and ~ 3 is larger by a factor of 2 and 4, respectively, than the present rate.
- In ellipticals, the chemical enrichment takes place so early that the metallicity effect on SNe Ia is not effective. Thus the SN Ia rate depends almost only on the lifetime. Our model (red solid line) includes the RG+WD systems with $t_{\text{Ia}} \gtrsim 10$ Gyr as the SN Ia progenitors, and thus the observed SN Ia rate in ellipticals can be well reproduced. Toward higher redshift, the predicted SN Ia rate does not change very much.
- In the K98 model (see Fig. 5 in K00), the lifetime distribution shows a gap between the two components of the MS+WD and RG+WD systems (Fig. 1), so that two peaks are clearly seen in the SN Ia rate in ellipticals. In our new SN Ia model, such peaks are not clearly seen (Fig. 3), because the lifetime ranges get gradually wider for higher metallicity.

4.2. SN Ia rate depending on Galaxy Type

Since the star formation history is different for different types of galaxies, the SN Ia and II rates depend on the morphological type of galaxies. In the observations, the present rates are available for various types of galaxies, which can give a constraint on the SN Ia models. In Figure 4 of K00, the observed ratio between SN Ia and II rates have been reproduced with our SN Ia model. The observational data is recently updated (Mannucci et al. 2006). We should note, however, that the absolute rates per B-band luminosity involves an uncertainty from dust extinction, and the rates per mass involves an uncertainty in the mass-to-light ratio.

We update the evolution models of four types of spiral galaxies, in order to meet the observational constraints on the present colors and the gas fractions, assuming the galactic age of 13 Gyr. The adopted infall and star formation timescales (see K00 for the definition) are summarized in Table 5. Figure 8 shows the time evolution of (a) the SFR, (c) the gas fraction per luminosity, and (d) the B-V color for four types of spirals (red dotted line for S0a/Sa; yellow solid line for Sab/Sb; green long-dashed line for Sbc/Sc; blue short-dashed line for Scd/Sd). In earlier-type of spirals, star formation takes place earlier, and thus the earlier-type of spirals have older ages of stellar populations, smaller gas fractions, and redder colors at present. In the panel (b), the upper and lower four lines respectively show the SN II and Ia rates per B-band luminosity (the supernova units, SNU). The observational data

is taken from Cappellaro et al. (1999) for S0a-Sb and Sbc-Sd. The present SN II+Ibc rate is larger for later-type of spirals, while the SN Ia rate in SNU is not different so much among the various types of galaxies, which are roughly consistent with the observation.

Figure 9 shows the present supernova rates per K-band luminosity (upper panel) and per mass (lower panel) against the morphological type of galaxies. The supernova rates are larger for later-type of spirals because the SFR is higher. Almost parallel relations between the observed rate and the galaxy type are seen for SNe II and Ibc, which may suggest the binary fraction is universal being independent of the galaxy type. Among core-collapse supernovae, we assume that 85% and 15% are SNe II (blue dashed line) and SNe Ibc (green dotted line), respectively. Thus, it may be reasonable to adopt the same b parameters as SNe Ia for all types of galaxies. As a result, our SN Ia model (red solid line) gives excellent agreement with the observed SN Ia rates. In our SN Ia models, there are two types of progenitor systems; The SN Ia rate is larger for later-type spirals, which is due to the young population of the MS+WD systems. The slope of the SN Ia rate against the galaxy type is flatter than that of the SN II and Ibc rates, which is due to the old population of the RG+WD systems.

The observational data is taken from Mannucci et al. (2006), where the adopted mass-to-light ratios are $M/L_K \sim 0.8, 0.7, 0.5$, and 0.4 for E/S0, S0a/b, Sbc/d, and Irr in their Table 2. In our models, the “stellar” mass-to-light ratios are $M/L_K \sim 1.29, 1.14, 1.07$, and 1.03 for S0a/Sa, Sab/Sb, Sbc/Sc, and Scd/Sd, which are ~ 2 times larger than their ratios. This difference might come from the difference in the IMF. We thus plot the observational data multiplied by a factor of 2 for the rates per mass.

Figure 10 compares the galactic supernova rates for different SN Ia models.

- In the DD model (green short-dashed line), the lifetime of the majority of SNe Ia is short, no large difference between the SN II and Ia rates is seen in the trend against the galaxy type, which is not consistent with the observations.
- The MR01 model (blue long-dashed line) and our SD models (red solid line and cyan dotted line) give almost the same trends, regardless of the metallicity effect, as far as the lifetime distributions in this work and K98 are applied.

4.3. Cosmic Supernovae Rate

Galaxies have different timescales for star formation and chemical enrichment, and the occurrence of SNe Ia depends on the metallicity therein. We calculate the cosmic supernova rate by summing up the supernova rates in spirals and ellipticals with the ratios of the

relative mass contribution in the Universe (see K00 for the detail). In Figure 6 of K00, the resultant cosmic SFRs shows a peak at $z \sim 2$. Figure 11 shows the cosmic supernova rates with our new SN Ia model, as a composite of those in spirals (blue long-dashed lines) and ellipticals (red short-dashed lines) in the supernova unit (upper panel) and in the unit of the comoving density (lower panel), respectively. The SN II rate (green dot-dashed lines) traces the star formation history, and shows a peak at $z \sim 2$ in the comoving density, being consistent with the observations (Cappellaro et al. 2005; Botticella et al. 2007).

As in spirals, the total SN Ia rate (green solid lines) gradually decreases toward $z \sim 2.6$ in the unit per luminosity, while the total SN Ia rate slightly increases to $z \sim 1$ and then decreases in the unit per volume. In ellipticals, the chemical enrichment takes place so quickly that the metallicity is large enough to produce SNe Ia at $z \gtrsim 2$. These are broadly consistent with the observations (e.g., Dahlen et al. 2004). Since the total SFR at $z \sim 0.5$ is smaller than observed, the total SN Ia rate seems to be smaller than observed.

Figures 12 and 13 show the cosmic SN Ia rate history for different SN Ia models.

- In the DD (short-dashed lines) and MR01 (long-dashed lines) models, the lifetime of the majority of SNe Ia is so short that the rate in ellipticals keeps on increasing at $z \lesssim 4$, and that the rate in spirals shows a peak at $z \sim 1.5$. As a result, the total SN Ia rate per luminosity is almost constant, and the rate per volume keeps on increasing toward higher redshifts. The total SN Ia rate is larger than the present rate by a factor of ~ 2 and ~ 4 at $z \sim 1$ and 2 , respectively.
- If we do not include the metallicity effect (dotted lines in Fig. 13), the SN Ia rate in spirals does not decrease so much, and the total SN Ia rate per luminosity is almost constant. The rate per volume slightly increases toward higher redshifts, and is larger than the present rate by a factor of ~ 2 at $z \sim 2$. In the observations, the decrease in the total rate is seen, which supports the existence of the metallicity effect.
- In the K98 model (see Fig. 6 in K00), two peaks are seen in the SN Ia rate history in ellipticals, which are not clearly seen in our new SN Ia model, because the lifetime ranges get gradually wider for higher metallicity (Fig. 3).

Note that this is a rough prediction of the cosmic supernova rates because several effects that should occur in the Universe are neglected; i) number evolution of each type of galaxies, ii) merging of galaxies, iii) internal structure, namely, the metallicity gradients within galaxies, iv) the contribution of dwarf galaxies. In the future work, we will show the cosmic supernova rates in the cosmological simulations (Kobayashi et al. 2007).

5. Discussion

5.1. SN Ia Formulation

In galactic chemical evolution models, the following two formulations have so far been proposed. Matteucci & Recchi (2001) argued that they could not reproduce K98 results. However, this is due to their misunderstanding of the parametrization of the K98 models as follows.

(1) The formulation of the SN Ia rate has been first proposed by Greggio & Renzini (1983) for the DD scenario, and extended for the SD scenario by Greggio (1996). This model is introduced as the “most popular” model by MR01. The SN Ia rate is described as

$$\mathcal{R}_{\text{Ia}} = A \int_{M_{\text{B,inf}}}^{M_{\text{B,sup}}} \phi(M_{\text{B}}) \int_{\mu_{\text{min}}}^{\mu_{\text{max}}} f(\mu) \psi(t - \tau_{M_2}) d\mu dM_{\text{B}}. \quad (1)$$

The first integral is for the total mass of the binary $M_{\text{B}} = M_1 + M_2$, and the second integral is for the mass fraction of the secondary star, $\mu = M_2/M_{\text{B}}$. The Scalo IMF ϕ is adopted in MR01, and the distribution function of the mass fraction is assumed as $f(\mu) = 2^{1+\gamma}(1+\gamma)\mu^\gamma$. $\gamma = 2$ is adopted in their successful models, which gives weight for massive secondaries in the distribution function of mass ratios (see Fig. 14). The upper and lower limits of integrals are $M_{\text{B,inf}} = \max[2M_2(t), M_{\text{Bm}}]$ and $M_{\text{B,sup}} = M_{\text{BM}}/2 + M_2(t)$, where the limits to the total mass of the binary are $M_{\text{Bm}} = 3M_\odot$ and $M_{\text{BM}} = 16M_\odot$. Therefore, the initial mass range of the primary stars is $1.5M_\odot - M_2 \leq M_1 \leq 8M_\odot$ and the secondary stars are AGB stars with the initial mass of $M_2 \leq 8M_\odot$. The lower limit of the primary, however, should not $1.5M_\odot$ but $\sim 3M_\odot$, since the primary should be a C+O WD. A denotes the fraction of binary stars, being set to be 0.05 in MR01.

(2) Based on the SD scenario, an alternative formulation has been proposed by K98 and K00. The SN Ia rate is given as

$$\mathcal{R}_{\text{Ia}} = b \int_{\max[m_{\text{p},\ell}, m_t]}^{m_{\text{p},u}} \frac{1}{m} \phi(m) dm \int_{\max[m_{\text{d},\ell}, m_t]}^{m_{\text{d},u}} \frac{1}{m} \psi(t - \tau_m) \phi_{\text{d}}(m) dm. \quad (2)$$

These integrals are calculated separately for the primary and secondary stars (m_{p} and m_{d}), respectively. The Salpeter IMF ϕ is adopted, and the distribution function of the companion’s mass is assumed to be the power-law as $\phi_{\text{d}}(m) \propto m^{-0.35}$. The slope -0.35 is chosen to meet the observation (Duguennoy & Mayor 1991), and such negative slope gives the distribution function weighted for less-massive secondaries (see Fig. 14). ϕ_{d} is normalized to unity in the integrated mass ranges as $\int_{m_{\text{d},\ell}}^{m_{\text{d},u}} \frac{1}{m} \phi_{\text{d}}(m) dm = 1$. Since the primary stars are C+O WDs, the initial mass range of the primary stars is $m_{\text{p}} = 3 - 8M_\odot$. The initial mass ranges of the

companion stars are given by the simulation of binary evolution (Hachisu et al. 1999ab), and are $m_d = 0.9 - 1.5M_\odot$ and $1.8 - 2.6M_\odot$ respectively for the RG+WD and MS+WD systems in K98. (In our new model (§2.2), the mass stripping effect is taken into account, and the mass ranges are updated as in Table 4.) The binary parameter b denotes the total fraction of primary stars that eventually produce SNe Ia, and is determined to reproduce the chemical evolution in the solar neighborhood. In K98, we adopted $b_{\text{RG}} = b_{\text{MS}} = 0.04$ from the Kolmogorov-Smirnov (KS) test of [O/Fe]-[Fe/H] relation in the solar neighborhood, but in K00, we adopted $[b_{\text{RG}}, b_{\text{MS}}] = [0.02, 0.05]$ from the χ^2 test¹. In addition, the metallicity effect is taken into account (see K98 and K00 for the details). The lowest metallicity to produce SNe Ia was set to be [Fe/H] = -1.1 both in K98 and K00².

The metallicity effect on SNe Ia can also be checked with the metallicity of the host galaxies of nearby SNe Ia. Three SNe Ia has been observed in low-metallicity dwarf galaxies; SN1895B and SN1972E in NGC 5253, and SN1937C in IC 4182. The metallicities of these galaxies are higher than [Fe/H] ~ -1 (K00). Hamuy et al. (2000) estimated the metallicities of host galaxies of 44 supernovae, and showed that no host galaxies found at [Fe/H] ~ -1 (Fig. 1 in Hamuy et al. 2001).

There is an uncertainty in the distribution function of the mass fraction $f(\mu)$ or the mass ratio $f(q)$ (Note that $q \equiv m_2/m_1 = \frac{\mu}{1-\mu}$ and $\frac{d\mu}{dq} = \frac{1}{(1+q)^2} = (1-\mu)^2$). In Figure 14, we show several forms of $f(q)$. The function that is introduced in MR01 is weighted for massive secondaries (i.e., the positive value of γ , long-dashed line). The observed distribution (histogram, Duguennoy & Mayor 1991) suggests that the function is weighted for less-massive secondaries, as in our function (solid line). Although our function $\phi_d(m_2)$ denotes the number function of secondary stars, we assume $\phi_d(m_2) \propto \phi(q)$ because the mass of primary stars (i.e., WDs) is almost constant of $\sim 1M_\odot$. It is, however, uncertain that initial mass ratios adopted in models is the same as the observed mass ratios. Among the binary population synthesis, several functions are adopted; $f(q) \propto (1+q)^{-2}$, i.e., constant $f(\mu)$ (dotted line, Portegies Zwart 1995), and constant $f(q)$, i.e., $f(\mu) \propto 1/(1-\mu)^2$ (short-dashed line, Han et al. 1995).

The IMF is also an assumption. For $m \geq 0.5M_\odot$, Kroupa (2007) shows a similar slope ($x = 1.3 \pm 0.5$) as the Salpeter IMF, which is flatter than the Scalo IMF. In chemical evolution models, metal enrichment is proceeded only by stars with $m \geq 0.5M_\odot$. Therefore, if a suitable value is chosen for the lower mass-cut of the IMF, the Salpeter IMF can give

¹There are two miss-prints in Appendix of K00, not $[b_{\text{MS}} = 0.02, b_{\text{RG}} = 0.05]$ but $[b_{\text{RG}} = 0.02, b_{\text{MS}} = 0.05]$.

²The note in MR01 is incorrect. See K98, $\ell.16$ in the right column, p.156, and K00, $\ell.15$ in the right column, p.27.

equal results with the Kroupa IMF. Therefore, we adopt the Salpeter IMF with a slope of $x = 1.35$ for a mass range of $m = 0.07 - 50M_{\odot}$.

5.2. [O/Fe]-[Fe/H] Relation

MR01 claimed that they failed to reproduce the K98 results (Mod.1 in MR01). Here we give counterargument by reproducing their and our results adopting their formula, Eq.[1]. We adopt, however, the same IMF, lifetime-mass relation, and nucleosynthesis yields as in our models (K06). We note that the analytical lifetime-mass relation adopted in MR01 gives shorter lifetimes for low-mass stars, because the metallicity effect on the stellar lifetime is not included. In Figure 15, the solid line shows our original K98 model, which can be reproduced even if we use the MR01 formula Eq.[1] (dotted line). Adopting their parameters, we can also reproduce Mod.1 and Mod.3 in MR01 (short- and long-dashed lines, respectively). It would be demonstrated that there was no error in K98. We then explain their misunderstandings about the following three points.

i) *Binary fraction* — The definition of b is different from that of A . In Eq.[2], b_{RG} and b_{MS} is the fraction of the progenitor WDs that eventually explode as SNe Ia for the RG+WD and MS+WD systems, respectively. b must be a combination of binary fraction A and some efficiency for each binary system, and could be determined from the binary population synthesis. However, since the evolution of binary systems are complicated and the effect of the WD winds are not included, we treat b as parameters and being determined for the RG+WD and MS+WD systems, independently, from the requirement to meet the observed MDF of G-dwarf stars in the solar neighborhood (Fig. 4c).

In Eq.[1], A denotes the binary fraction, which would be constrained from observations, and should be the same for the RG+WD and MS+WD systems from its definition. However, MR01 adopted $A = 0.02$ and 0.05 for the RG+WD and MS+WD systems, respectively, which are the same values of the binary parameter b in K00. Since ϕ_{d} is normalized to unity not for $m = 0.07 - 50M_{\odot}$ but for $m_{\text{d}} \sim 1 - 3M_{\odot}$, the value of A should be ten times larger than the value of b . If we adopt $A = 0.45$, we can derive almost the same results (dotted line) as K98 (solid line). With the MR01 formula Eq.[1], the slope of [O/Fe] is slightly different, and [O/Fe] around [Fe/H] ~ -0.5 is slightly higher than the K98 model. We also note that MR01 adopted $\gamma = -0.35$ to try to reproduce our results, but $\gamma = -1.35$ is correct, because the number function should be the mass function ϕ_{d} multiplied by $1/m$.

ii) *Mass fraction* — The suitable value of A depends on the distribution function of the mass fraction $f(\mu)$. In Figure 16, we show almost identical results with different sets

of A and $f(\mu)$. The parameter A is determined from the MDF in the solar neighborhood. This means that the uncertainty of $f(\mu)$ itself is not important. The solid line shows the K98 model calculated with the MR01 formula. Since $f(\mu)$ with $\gamma = -1.35$ is weighted for low-mass secondaries, the relative contribution of the MS+WD systems is small, and A is required to be as large as 0.45. With the constant $f(\mu)$ or constant $f(q)$, the contribution of the MS+WD systems is as large as that of the RG+WD systems, and thus A becomes 0.30 and 0.25, respectively. With $\gamma = 2$ as in MR01, $A = 0.20$ gives the best fit. The binary fraction of $A \sim 0.5$ might be too large, but $A \sim 0.2$ looks reasonable.

iii) *IMF* — There is another difference in the treatment of the IMF; the IMF is applied to the total mass of the binary in the MR01 model, while it is applied to the mass of the primary star in the K98 model. If we adopt not $\phi(m_B)$ but $\phi(m_1)$, the normalization is changed by a factor. For $\gamma = -1.35$, constant $f(\mu)$, constant $f(q)$, and $\gamma = 2$, A becomes 0.25, 0.15, 0.12, and 0.10, respectively.

6. Conclusions

We construct a new SN Ia model, based on the SD scenario for the SN Ia progenitors, taking account of the metallicity effect of the WD wind (K98) and the mass-stripping effect on the binary companion star (HKN07). The lifetime distribution of SNe Ia is determined from the main-sequence mass range of the companion stars in the WD binary systems, and is given as a function of metallicity. Our model naturally predicts that the SN Ia lifetime distribution spans a range of 0.1–20 Gyr with the double peaks at ~ 0.1 and 1 Gyr reflecting the two systems of the companion stars; the MS+WD and RG+WD systems, respectively.

We make a comparison of the lifetime distribution functions derived from different SN Ia models, and evaluate the results from the observational constraints as summarized in Table 6.

(1) Contrary to the argument in Matteucci & Recchi (2001, MR01), our SN Ia models give better reproduction of the $[\alpha/\text{Fe}]$ - $[\text{Fe}/\text{H}]$ relation in the solar neighborhood. In the DD and MR01 models, the typical lifetimes of SNe Ia are ~ 0.1 and 0.3 Gyr, respectively, which results in the too early decrease in $[\alpha/\text{Fe}]$ at $[\text{Fe}/\text{H}] \sim -2$. If we do not include the metallicity effect in our model, $[\alpha/\text{Fe}]$ decreases too early because of the shortest lifetime, ~ 0.1 Gyr, of the MS+WD systems. In other words, the presence of the young population of SNe Ia strongly favors the presence of the metallicity effect to be consistent with the chemical evolution of the solar neighborhood.

(2) At the same $[\text{Fe}/\text{H}]$, $[\text{Mn}/\text{Fe}]$ starts to increase toward higher metallicity, because SNe

Ia produce $[\text{Mn}/\text{Fe}] > 0$. This evolutionary change is started from the same $[\text{Fe}/\text{H}]$ as the decreasing trends of $[\alpha/\text{Fe}]$. $[\text{Zn}/\text{Fe}]$ evolves differently for the different SNe Ia models, because of the combination of the different lifetime of SNe Ia and the metallicity effect on Zn yields of SNe II. Further observations of these elements at $[\text{Fe}/\text{H}] \gtrsim -1.5$ is critically important in order to identify the SN Ia progenitors and to clarify the metallicity dependence on the nucleosynthesis yields.

(3) To explain the observed SN Ia in ellipticals at $z = 0$, the lifetimes of a sufficient fraction of SNe Ia should be longer than ~ 10 Gyr, which is satisfied in our SD model and the MR01 model, but not in the DD model. Our SN Ia models are also successful in reproducing the SN II, Ibc, and Ia rates with their dependence on the galaxy type (Mannucci et al. 2006); This cannot be reproduced with the DD model. The large SN Ia rate in radio galaxies could be explained with the young population of the MS+WD systems in our model.

(4) We also provide the cosmic supernova rate history as a composite of those in spirals and ellipticals. The cosmic SN Ia rate in comoving density shows a peak at $z \sim 1$ and decreases toward higher redshift in our model. In contrast, this rate increases toward higher redshifts in the DD and MR01 models. Because of the metallicity effect, i.e., because of the lack of winds from WDs in the binary systems at $[\text{Fe}/\text{H}] \lesssim -1$, the SN Ia rate in the low-metallicity systems, e.g., high- z spiral galaxies, is supposed to be very small in our model. In contrast, the SN Ia rate in such systems is as high as present in the DD and MR01 models. In our models, at $z \gtrsim 1$, SNe Ia will be observed only in the systems that have evolved with a short timescale of chemical enrichment. This suggests that the evolution effect in the supernova cosmology can be small.

This work has been supported in part by the Grant-in-Aid for Scientific Research (18104003, 18540231) and the 21st Century COE Program (QUEST) from the Japan Society for Promotion of Science (JSPS) and the Ministry of Education, Culture, Sports, Science, and Technology (MEXT) of Japan, and also by the National Science Foundation under Grant No. PHY05-51164 at Kavli Institute for Theoretical Physics of USA. C.K. thank to the JSPS for a financial support. We would like to thank I. Hachisu, M. Kato, M. Tanaka, F. Matteucci, S. Recchi, M. Della Valle, P. Podsiadlowski, R. Ellis, L. Greggio, and A. Renzini for fruitful discussion. We are particularly grateful to the late Prof. B. E. J. Pagel for generous suggestion and encouragement.

REFERENCES

Arnett, W. D. 1996, *Supernovae and Nucleosynthesis* (Princeton Univ. Press)

- Barris, B. J. & Tonry, J. L. 2006, *ApJ*, 637, 427
- Bensby, T., Feltzing, S., Lundström, I. 2003, *A&A*, 410, 527
- Bensby, T., Feltzing, S., Lundström, I. 2004, *A&A*, 415, 155
- Blanc, G. et al. 2004, *A&A*, 423, 881
- Boesgaard, A. M., King, J. R., Deliyannis, C. P., Vogt, S. S. 1999, *AJ*, 117, 492
- Botticella, M. T. et al. 2007, *astro-ph/0710.3763*
- Canal, R., Méndez, J., & Ruiz-Lapuente, P. 2001, *ApJ*, 550, L53
- Cappellaro, E., Evans, R., & Turatto, M. 1997, *A&A*, 351, 459
- Cappellaro, E., et al. 2005, *A&A*, 430, 83
- Cayrel, R. et al. 2004, *A&A*, 416, 1117
- Dahlen, T. et al. 2004, *ApJ*, 613, 189
- Della Valle, M., Panagia, N., Padovani, P., Cappellaro, E., Mannucci, F., & Turatto, M. 2005, *ApJ*, 629, 750
- Duguennoy, A., & Mayor, M. 1991, *A&A*, 248, 485
- Edvardsson, B., Andersen, J., Gustafsson, B., Lambert, D. L., Nissen, P. E., & Tomkin, J. 1993, *A&A*, 275, 101
- Filippenko, A.V. 1997, *ARA&A*, 35, 309
- Geier, S., Nesslinger, S., Heber, U., Przybilla, N., Napiwotzki, R., Kudritzki, R.-P. 2007, *A&A*, 464, 299
- Gratton 1989, *A&A*, 208, 171
- Gratton, R. G. et al. 2003, *A&A*, 404, 187
- Greggio, L. 1996, in *The Interplay between Massive Star Formation, the ISM, and Galaxy Evolution*, ed. D. Kunth et al. (Gif-suf-Yvette: Edition Frontières), 98
- Greggio, L. 2005, *A&A*, 441, 1055
- Greggio, L. & Renzini, A. 1983, *A&A*, 118, 217
- Hachisu, I., Kato, M., & Nomoto, K. 1996, *ApJ*, 470, L97
- Hachisu, I., Kato, M., & Nomoto, K. 1999a, *ApJ*, 522, 487
- Hachisu, I., Kato, M., Nomoto, K., & Umeda, H. 1999b, *ApJ*, 519, 314
- Hachisu, I., Kato, M., & Nomoto, K. 2007, *ApJ*, submitted, *astro-ph/0710.0319* (HKN07)
- Hamuy, M., Trager, S. C., Pinto, P. A., Phillips, M. M., Schommer, R. A., Ivanov, V. & Suntzeff, N. B. 2000, *AJ*, 120, 1479
- Hamuy, M., Trager, S. C., Pinto, P. A., Phillips, M. M., Schommer, R. A., Ivanov, V. & Suntzeff, N. B. 2001, *AJ*, 122, 3506

- Hamuy, M. & Pinto, P. A. 1999, *AJ*, 117, 1185
- Han, Z., Eggleton, P. P., Podsiadlowski, P. & Tout, C. A. 1995, *MNRAS*, 277, 1443
- Hardin, D. et al. 2000, *A&A*, 362, 419
- Hillebrandt, W. & Niemeyer, J. C. 2000, *ARA&A*, 38, 191
- Höflich, P., & Khokhlov, A. 1996, *ApJ*, 457, 500
- Honda, S. et al. 2004, *ApJ*, 607, 474
- Iben, I. Jr., & Tutukov, A. V. 1984, *ApJS*, 54, 335
- Israelian, Garcia-Lopez, Rebolo 1998, *ApJ*, 207, 805
- Kobayashi, C., & Arimoto, N. 1999, *ApJ*, 527, 573
- Kobayashi, C., Springel, V., & White, S. D. M. 2007, *MNRAS*, 376, 1465
- Kobayashi, C., Tsujimoto, T., & Nomoto, K. 2000, *ApJ*, 539, 26 (K00)
- Kobayashi, C., Tsujimoto, T., Nomoto, K., Hachisu, I., & Kato, M. 1998, *ApJ*, 503, L155 (K98)
- Kobayashi, C., Umeda, H., Nomoto, K., Tominaga, N., & Ohkubo, T. 2006, *ApJ*, 653, 1145 (K06)
- Kroupa, P. 2007, ASP Conference Series, in press, astro-ph/0708.1164
- Kuznetsova, N. et al. 2007, astro-ph/0710.3120
- Livio, M. 2001, in *Supernovae and Gamma-Ray Bursts*, eds. M. Livio et al. (New York: Cambridge University Press), 334
- Madgwick, D. S., Hewett, P. C., Mortlock, D. J., & Wang, L. 2003, *ApJ*, 599, L33
- Mannucci, F., Della Valle, M., & Panagia, N. 2006, *MNRAS*, 370, 773
- Matteucci, F. 1997, in ASP Conference Series, Vol. 126, *From Quantum Fluctuations to Cosmological Structures*, 495
- Matteucci, F. 2001, *The Chemical Evolution of the Galaxy* (Kluwer Academic Pub.)
- Matteucci, F., & Greggio, L. 1986, *A&A*, 154, 279
- Matteucci, F., Panagia, N., Pipino, A., Mannucci, F., Recchi, S. & Della Valle, M 2006, *MNRAS*, 372, 265
- Matteucci, F. & Recchi, S. 2001, *ApJ*, 558, 351 (MR01)
- McWilliam, A., Preston, G.W., Sneden, C., & Searle, L. 1995, *AJ*, 109, 2757
- Napiwotzki, R., et al. 2005, AIP Conference Proceedings, Vol. 804, 173, astro-ph/0509801
- Napiwotzki, R. 2007 talk at the KITP workshop on Paths to Exploding Stars: Accretion and Eruption, Santa Barbara, 19-23 March, http://online.kitp.ucsb.edu/online/snovae_c07

- Neil, J. D. et al. 2006, *ApJ*, 132, 1126
- Nissen, P. E., Chen, Y. Q., Asplund, M., & Pettini, M. 2004, *A&A*, 415, 993
- Nomoto, K., Iwamoto, K., & Kishimoto, N. 1997, *Science*, 276, 1378
- Nomoto, K., Saio, H., Hachisu, I. & Kato, M. 2007, 663, 1269
- Nomoto, K., Tominaga, N., Umeda, H., Kobayashi, C, & Maeda, K. 2006, *Nuclear Physics A*, 777, 424
- Nomoto, K., Umeda, H., Hachisu, I., Kako, M., Kobayashi, C., & Tsujimoto, T. 2000, in *Type Ia Supernovae: Theory and Cosmology*, eds. J. Niemeyer & J. Truran (New York: Cambridge University Press), 63 (astro-ph/9907386)
- Nomoto, K., Yamaoka, H., Shigeyama, T., Kumagai, S., & Tsujimoto, T. 1994, in *Supernovae, Les Houches Session LIV*, ed. S. A. Bludman et al. (Amsterdam: North-Holland), 199
- Nordström, B., Mayor, M., Andersen, J., Holmberg, J., Pont, F., Jorgensen, B. R., Olsen, E. H., Udry, S., Mowlavi, N. 2004, *A&A*, 418, 989
- Nugent, P., Baron, E., Branch, D., Fisher, A., & Hauschildt, P. H. 1997, *ApJ*, 485, 812
- Pagel, B. E. J. 1997, *Nucleosynthesis and Chemical Evolution of Galaxies* (Cambridge Univ. Press)
- Pain, R., et al. 1996, *ApJ*, 473, 356
- Pain, R., et al. 2002, *ApJ*, 577, 120
- Portegies Zwart, S. F. 1995, *A&A*, 296, 691
- Primas, F., Brugamyer, E., Sneden, C., King, J. R., Beers, T. C., Boesgaard, A. M., Deliyannis, C. P. 2000, in *The First Stars*, eds. A. Weiss, T. Abel, & V. Hill (Berlin: Springer), 51
- Riess, A. 1996, Ph.D thesis, Harvard University
- Roberts, M. S. & Haynes, M. P. 1994, *ARA&A*, 32, 115
- Ryan, S. G., Norris, J. E., & Beers, T. C. 1996, *ApJ*, 471, 254
- Saio, H., & Nomoto, K. 1985, *A&A*, 150, L21
- Saio, H., & Nomoto, K. 1998, *ApJ*, 500, 388
- Scannapieco, E. & Bildsten, L. 2005, *ApJ*, 629, L85
- Sneden, C., Gratton, R. G., & Crocker, D. A. 1991, *A&A*, 246, 354
- Strolger, L.-G. et al. 2004, *ApJ*, 613, 200
- Sullivan, M. et al. 2006, *ApJ*, 648, 868
- Tonry, J. L. et al. 2003, *ApJ*, 594, 1
- Tutukov, A. V., & Yungelson, L. R. 1994, *MNRAS*, 268, 871

- Umeda, H. & Nomoto, K. 2002, *ApJ*, 565, 385
- Webbink, R. F. 1984, *ApJ*, 277, 355
- Wyse, R. F. G., & Gilmore, G. 1995, *AJ*, 110, 2771
- Yoshii, Y., Tsujimoto, T., & Kawara, K. 1998, *ApJ*, 507, 113
- Yungelson, L. R., Lasota, J.-P., Nelemans, G., Dubus, G., van den Heuvel, E. P. J., Dewi, J., & Portegies Zwart, S. 2006, *A&A*, 454, 559
- Yungelson, L. R. 2005, in: *White dwarfs: cosmological and galactic probes*, eds. E. M. Sion, S. Vennes & H. L. Shipman (Dordrecht: Springer), 163
- Yungelson, L., & Livio, M. 1998, *ApJ*, 497, 168

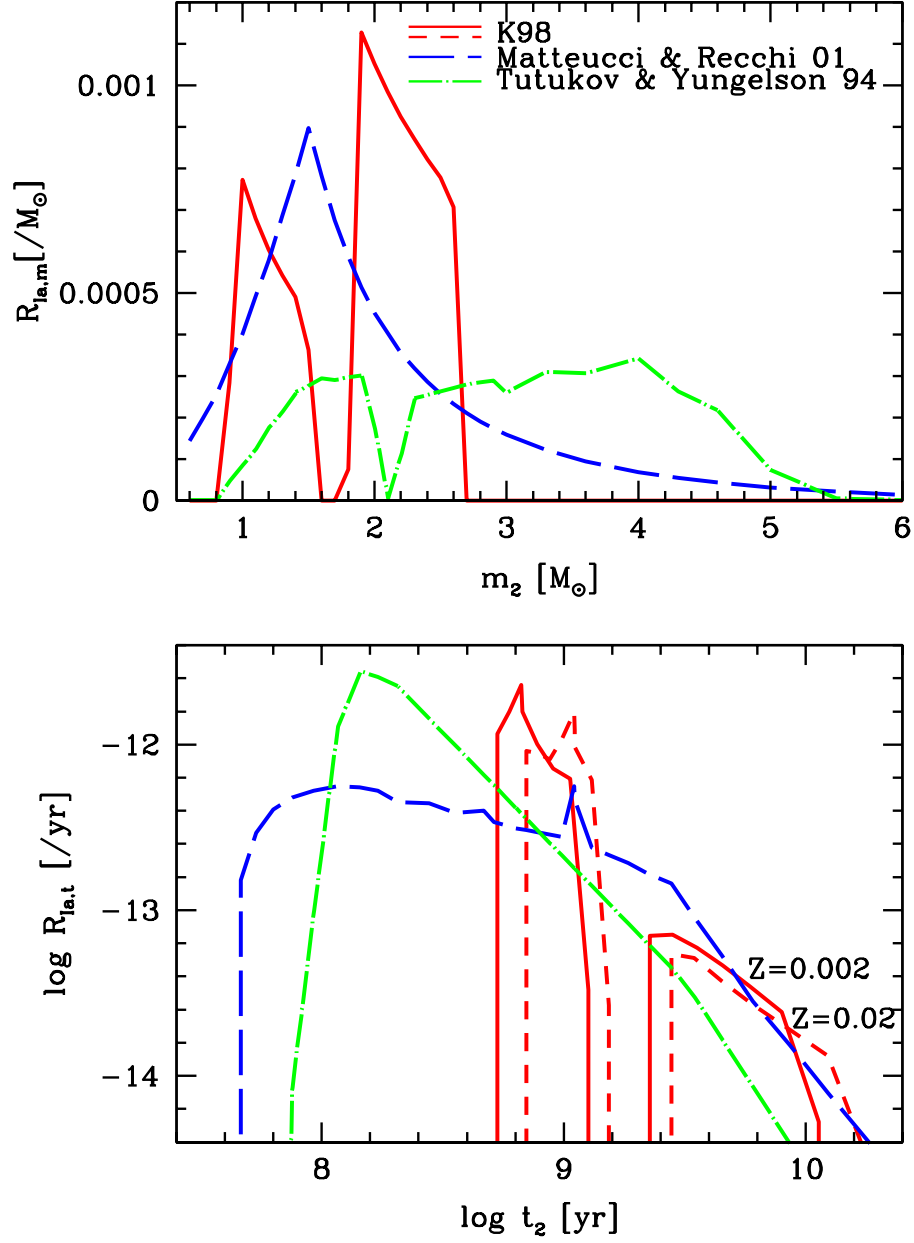


Fig. 1.— The distribution functions of the progenitor mass (upper panel) and lifetime (lower panel), i.e., the SN Ia rates of stars with the same ages, for K98 model with $Z = 0.002$ (red solid line) and $Z = 0.02$ (red short-dashed line), MR01 model (blue long-dashed line, Matteucci & Recchi 2001), and DD model (green dot-dashed line, Tutukov & Yungelson 1994).

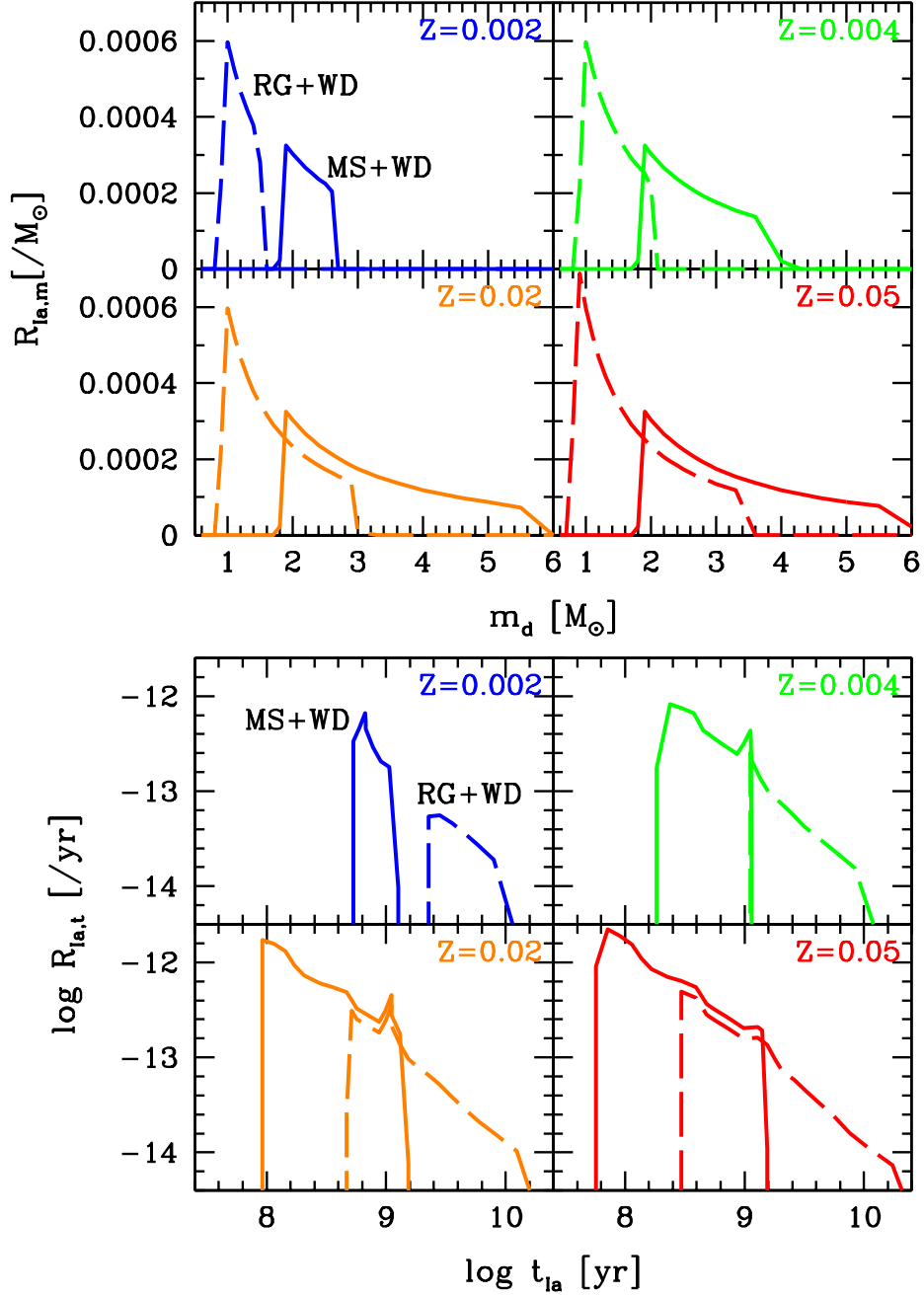


Fig. 2.— The distribution functions of the progenitor mass (upper panel) and lifetime (lower panel) for the metallicity $Z = 0.002$ (blue), 0.004 (green), 0.02 (orange), and 0.05 (red). The solid and dashed lines indicate the MS+WD and RG+WD systems, respectively, that correspond to the young and old population of SNe Ia.

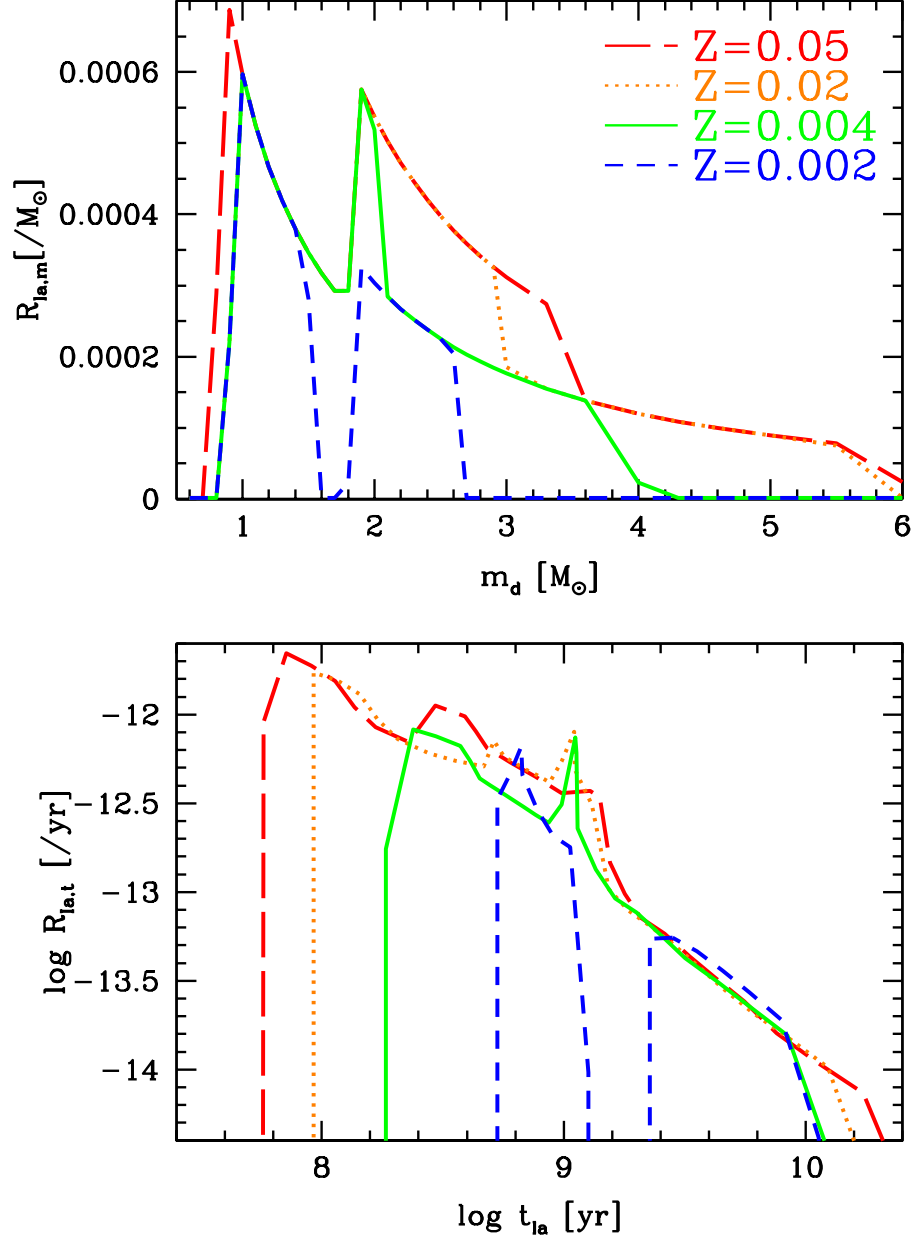


Fig. 3.— The distribution functions of the progenitor mass (upper panel) and lifetime (lower panel), i.e., the SN Ia rates of stars with the same ages, for our new models with the metallicity $Z = 0.002$ (blue short-dashed line), $Z = 0.004$ (green solid line), $Z = 0.02$ (orange dotted line), and $Z = 0.05$ (red long-dashed line).

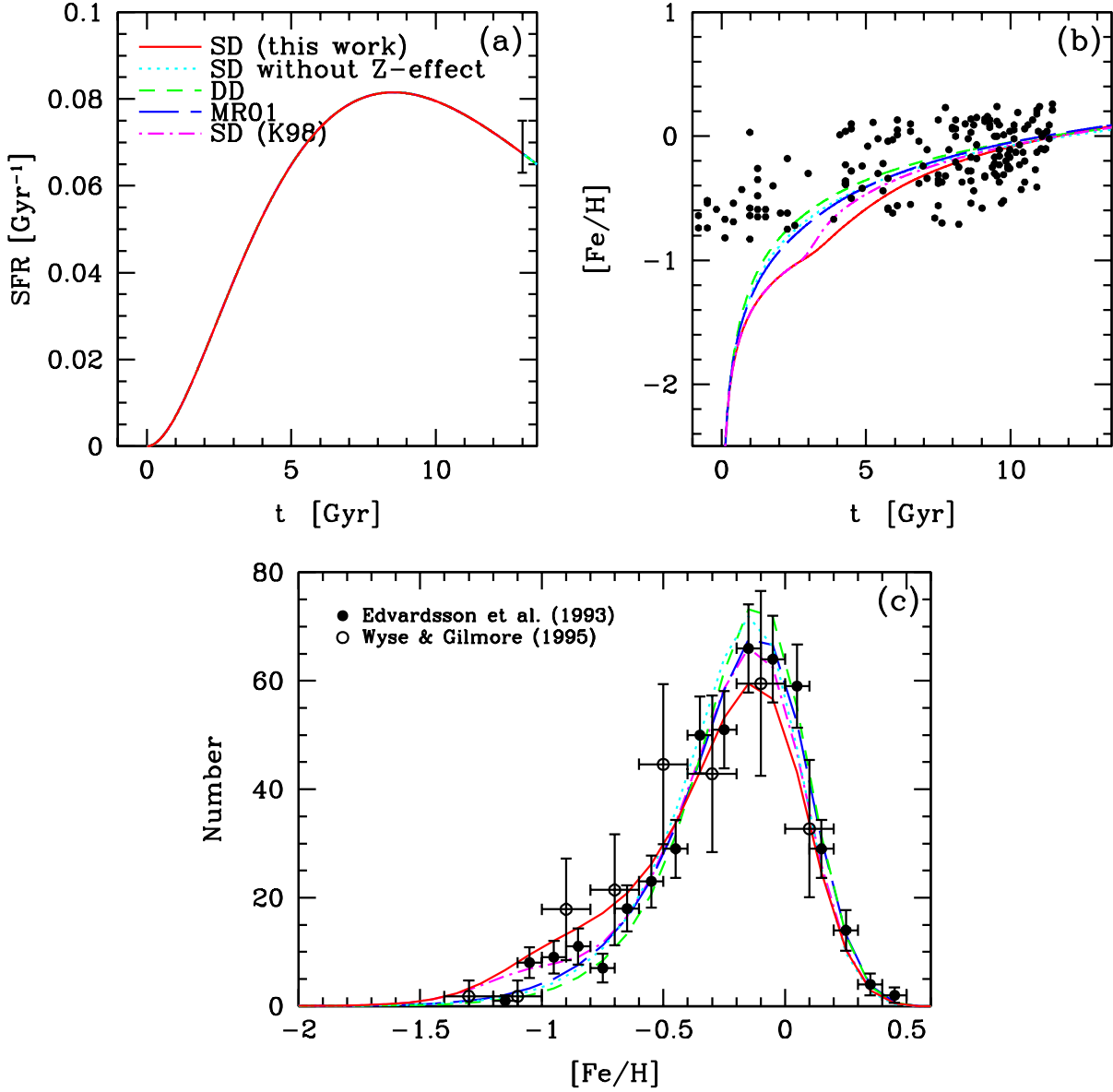


Fig. 4.— The chemical evolution of the solar neighborhood; (a) the star formation rate, (b) the age-metallicity relation, and (c) the metallicity distribution function for different SN Ia models; our SD model (red solid line), SD model without metallicity effect (cyan dotted line), DD model (green short-dashed line), MR01 model (blue long-dashed line), and K98 model (magenta dot-dashed line). Observational data sources are: Matteucci (1997), errorbar in panel (a); Edvardsson et al. (1993), filled circles in panels (b) and (c); Wyse & Gilmore (1995), open circles in panel (c).

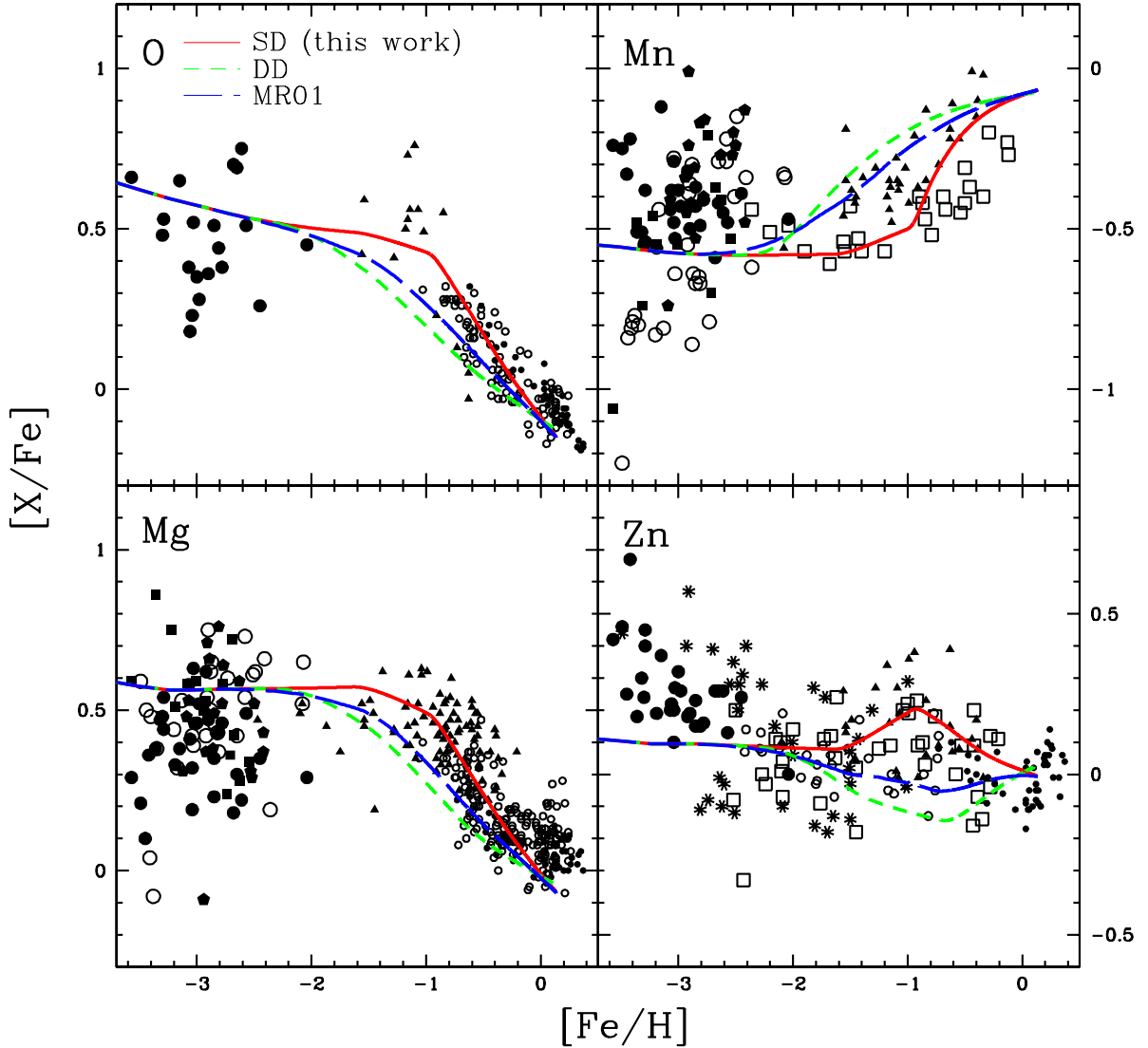


Fig. 5.— The evolution of the elemental abundance ratios, $[X/Fe]$ - $[Fe/H]$ relations, in the solar neighborhood for different SN Ia model; our SD model (red solid line), DD model (green short-dashed line), and MR01 model (blue long-dashed line). Observational data sources are: For disk stars, Edvardsson et al. (1993), small open circles; thin disk stars in Bensby et al. (2003, 2004), small filled circles; accretion component in Gratton et al. (2003), triangles. For halo stars, McWilliam et al. (1995), large open circles; Ryan et al. (1996), filled squares; Cayrel et al. (2004), large filled circles; Honda et al. (2004), filled pentagons. For Mn, Gratton (1989), open squares. For Zn, Sneden et al. (1991), open squares; Primas et al. (2000), eight-pointed asterisks; Nissen et al. (2004), open circles.

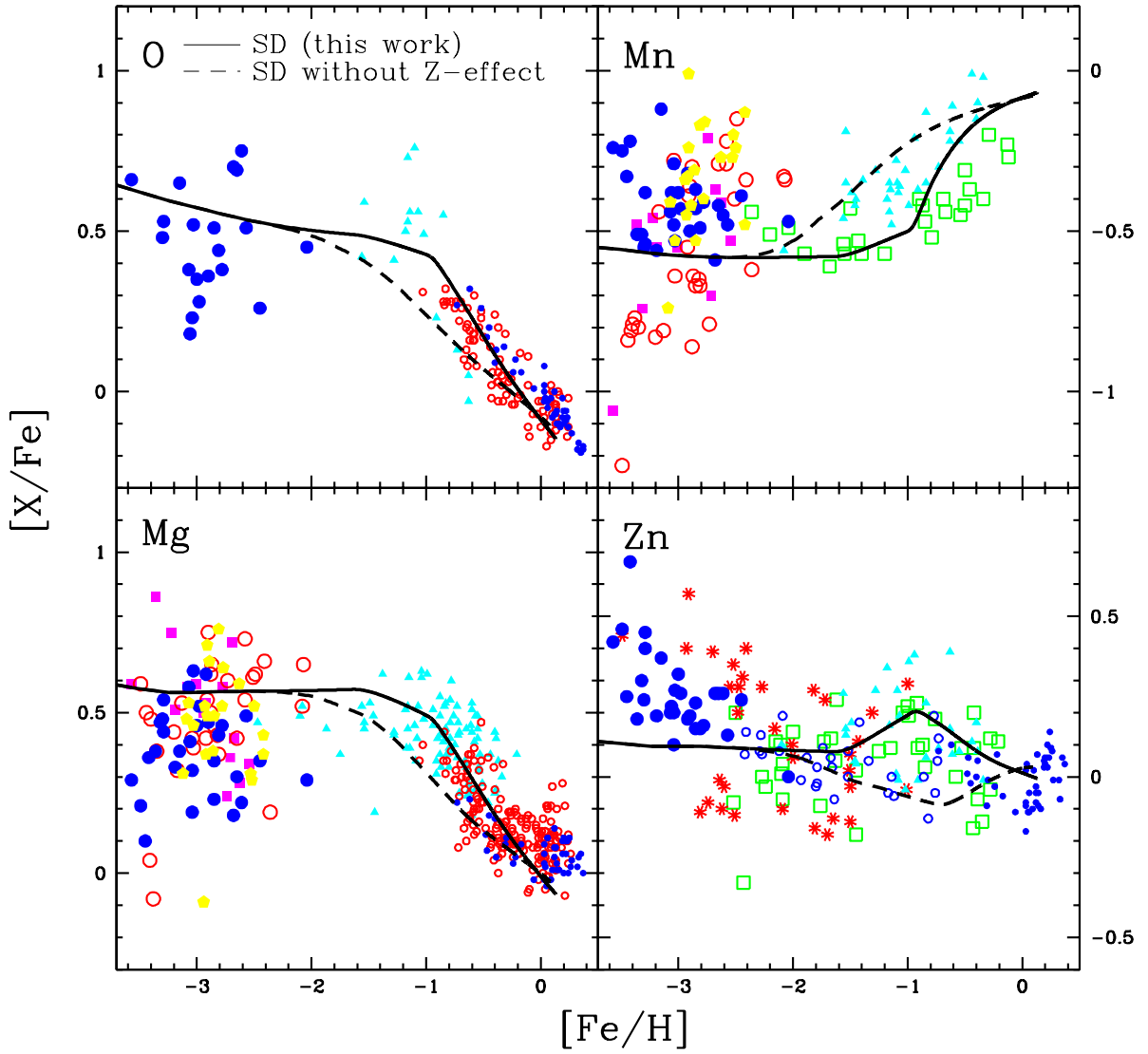


Fig. 6.— Same as Figure 5 but for our SD model with (solid line) and without (dotted line) metallicity effect.

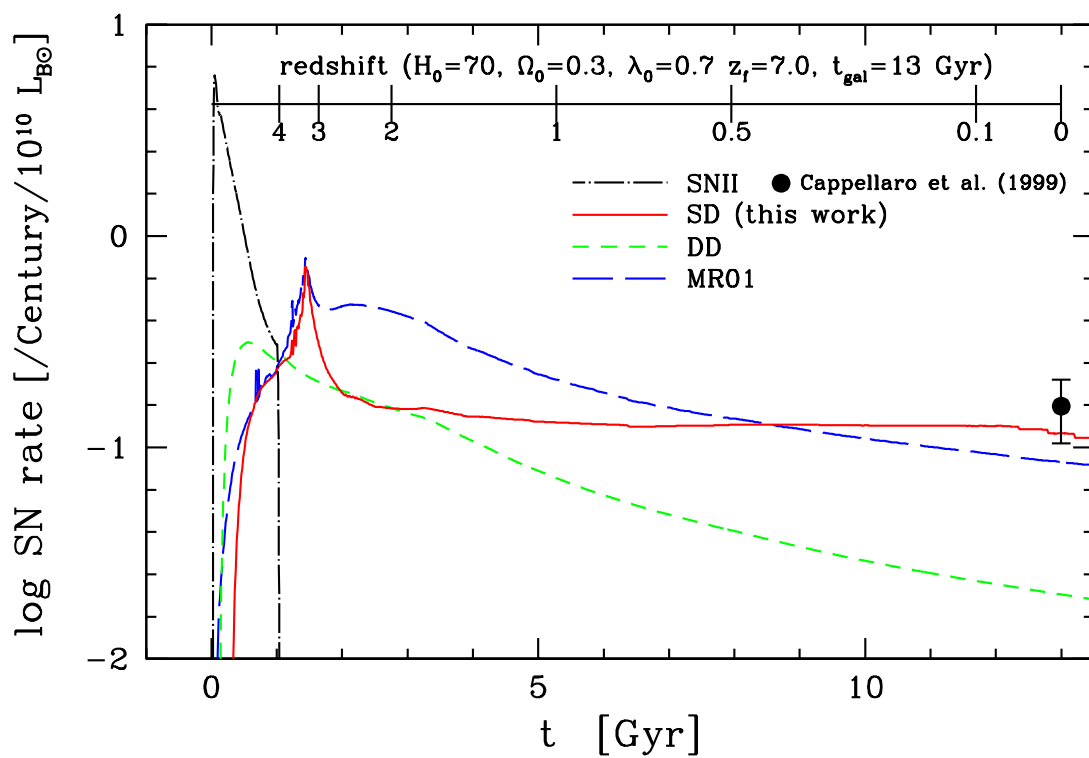


Fig. 7.— The SN Ia rate history in ellipticals for different SN Ia models; our SD model (red solid line), DD model (green short-dashed line), and MR01 model (blue long-dashed line). The dot-dashed line shows the SN II rate. The observational data is taken from Cappellaro et al. (1999).

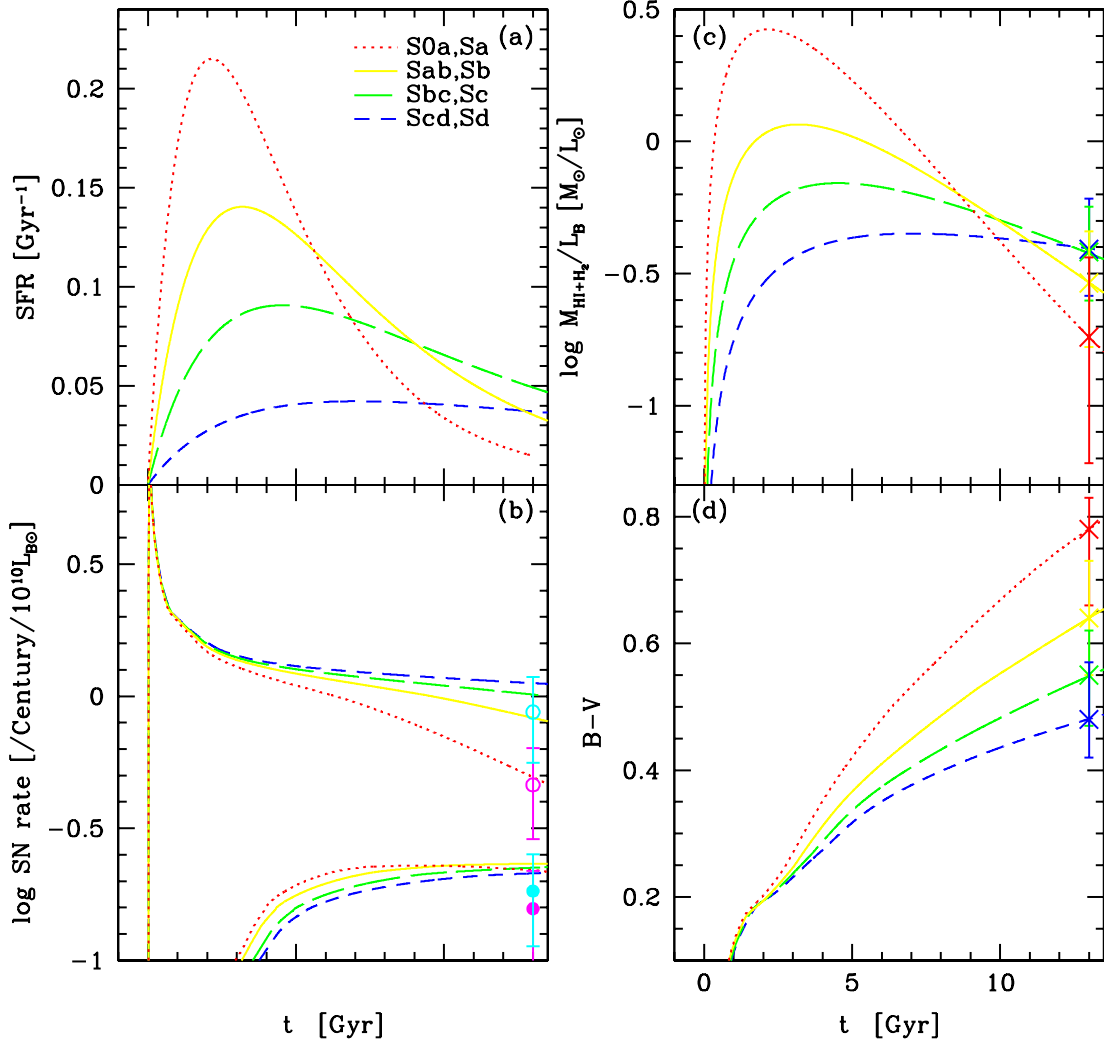


Fig. 8.— The time evolution of (a) the SFR, (b) the SN II and Ia rates, (c) the gas fraction per luminosity, and (d) the B-V color for four types of spirals (red dotted line, S0a/Sa; yellow solid line, Sab/Sb; green long-dashed line, Sbc/Sc; blue short-dashed line, Scd/Sd). In the panel (b), the upper and lower four lines are for the SN II and Ia rates per B-band luminosity (the supernova units, SNU), respectively. The observational data sources are: Matteucci (1997) (panel a), Cappellaro et al. (1999) for S0a-Sb and Sbc-Sd (panel b), and Roberts & Haynes (1994) (panels c and d).

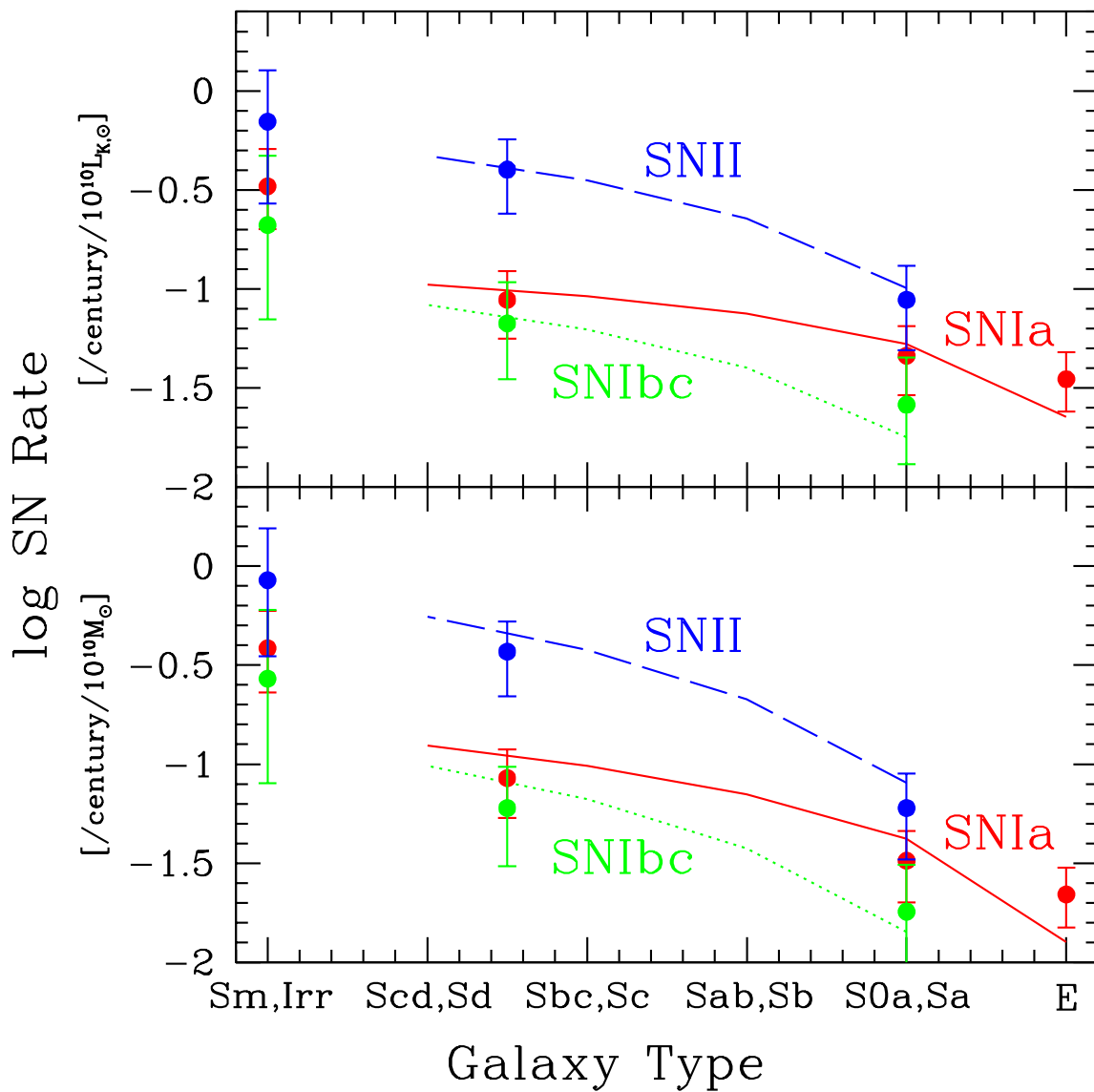


Fig. 9.— The present supernova rates per K-band luminosity (upper panel) and per mass (lower panel) against the morphological type of galaxies for SNe II (blue dashed line), Ia (red solid line), and Ibc (green dotted line).

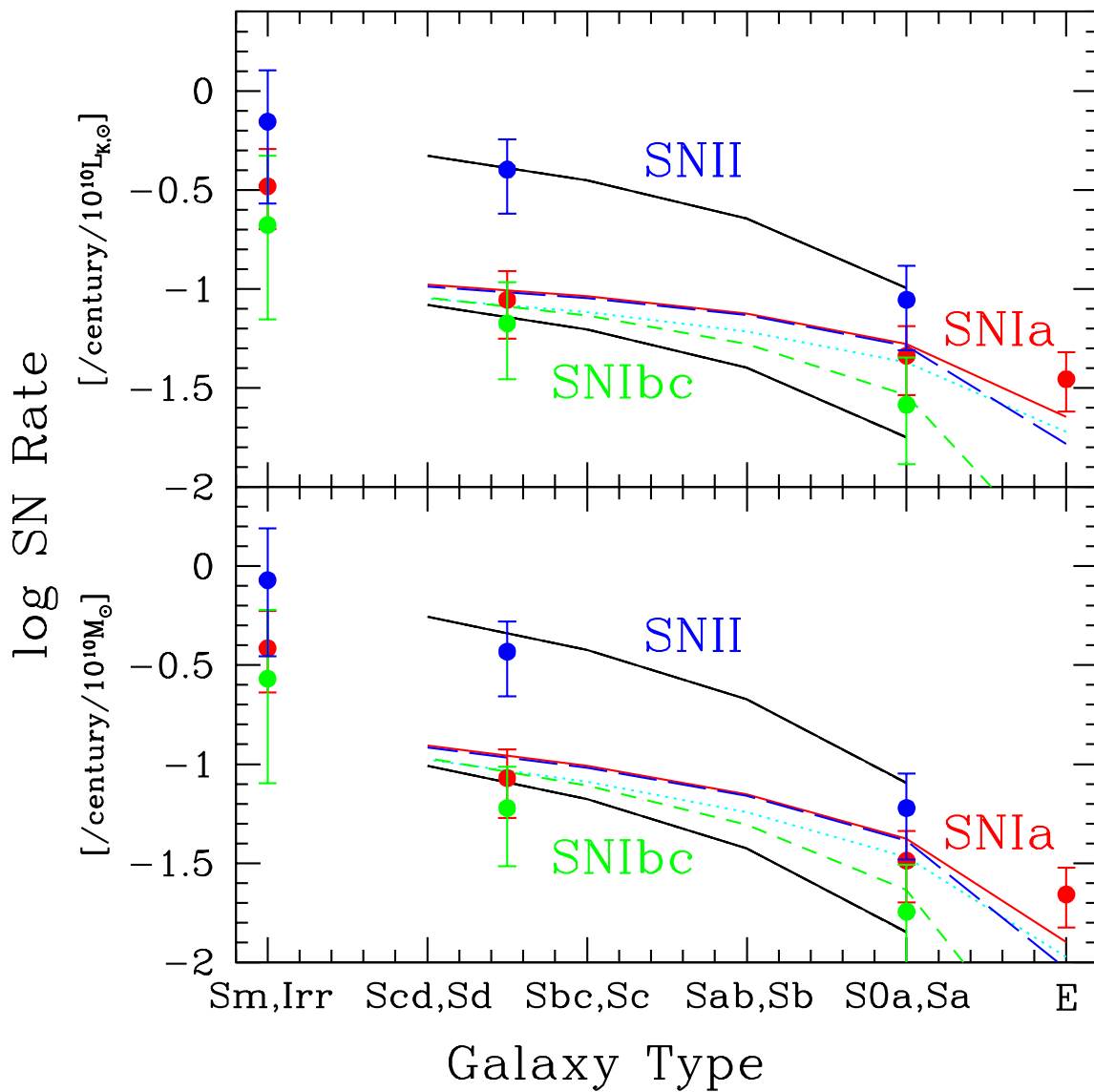


Fig. 10.— Same as Figure 9, but for different SN Ia models; our SD model with (red solid line) and without (cyan dotted line) metallicity effect, DD model (green short-dashed line), and MR01 model (blue long-dashed line).

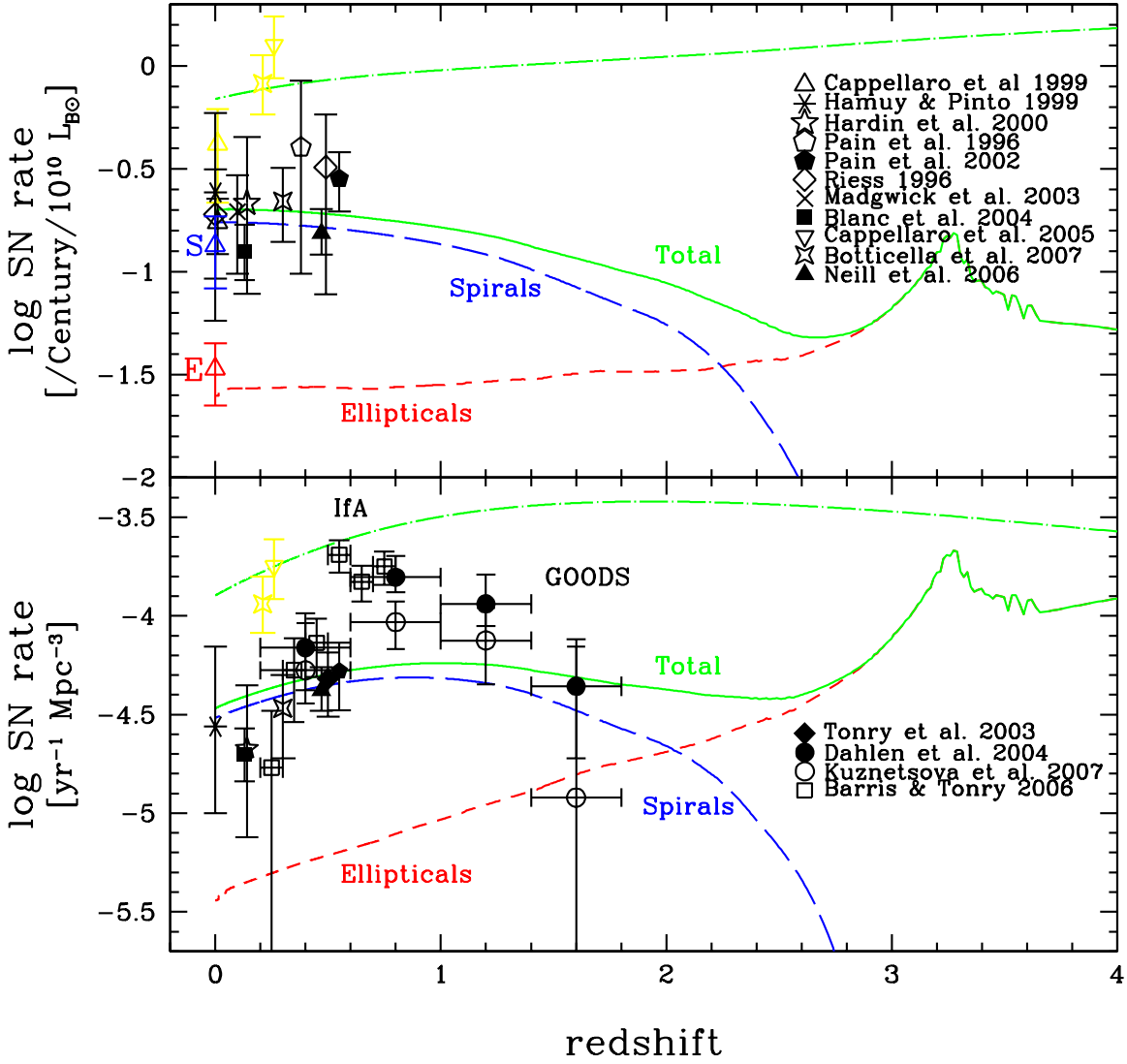


Fig. 11.— The cosmic supernova rates as a composite of those in spirals (blue long-dashed line) and ellipticals (red short-dashed line) in the supernova units (upper panel) and in the units of the comoving density (lower panel). The green solid and dot-dashed lines are for the SN Ia and II rates, respectively. Observational data sources are: Cappellaro et al. (1999), open triangles; Hamuy & Pinto (1999), asterisk; Hardin et al. (2000), star; Pain et al. (1996), open pentagon; Pain et al. (2002), filled pentagon; Riess (1996), open diamonds; Madgwick et al. (2003), cross; Blanc et al. (2004), filled square; Cappellaro et al. (2005), inverted open triangle; Botticella et al. (2007), four-pointed stars; Neil et al. (2006), filled triangle; Tonry et al. (2003), filled diamond; Dahlen et al. (2004), filled circles; Barris & Tonry (2006), open squares; Kuznetsova et al. (2007), open circles. The observational data of the core-collapse supernovae is shown with yellow color.

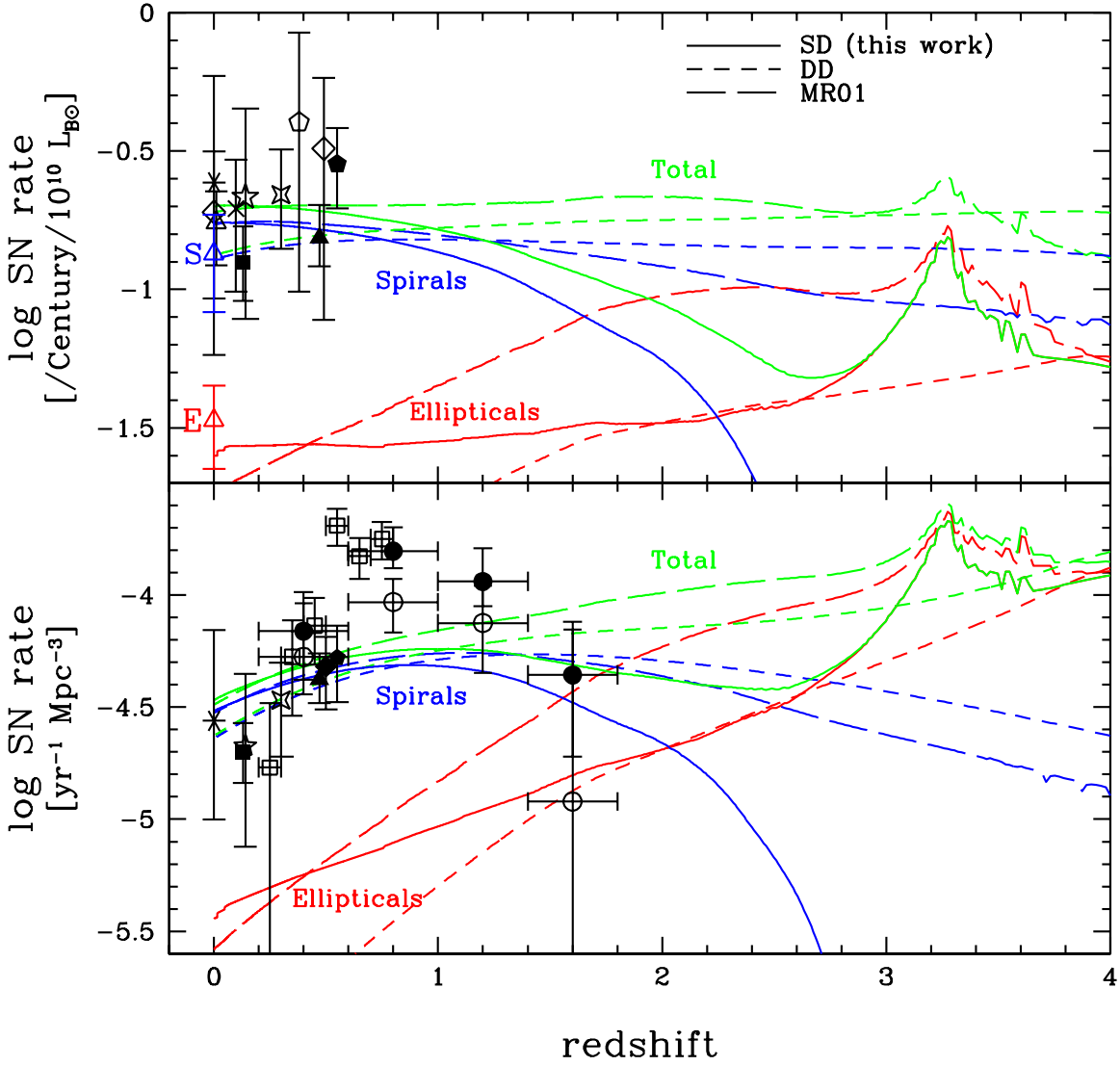


Fig. 12.— Same as Figure 11, but for different SN Ia models; our SD model with metallicity effect (solid lines), DD model (short-dashed lines), and MR01 model (long-dashed lines).

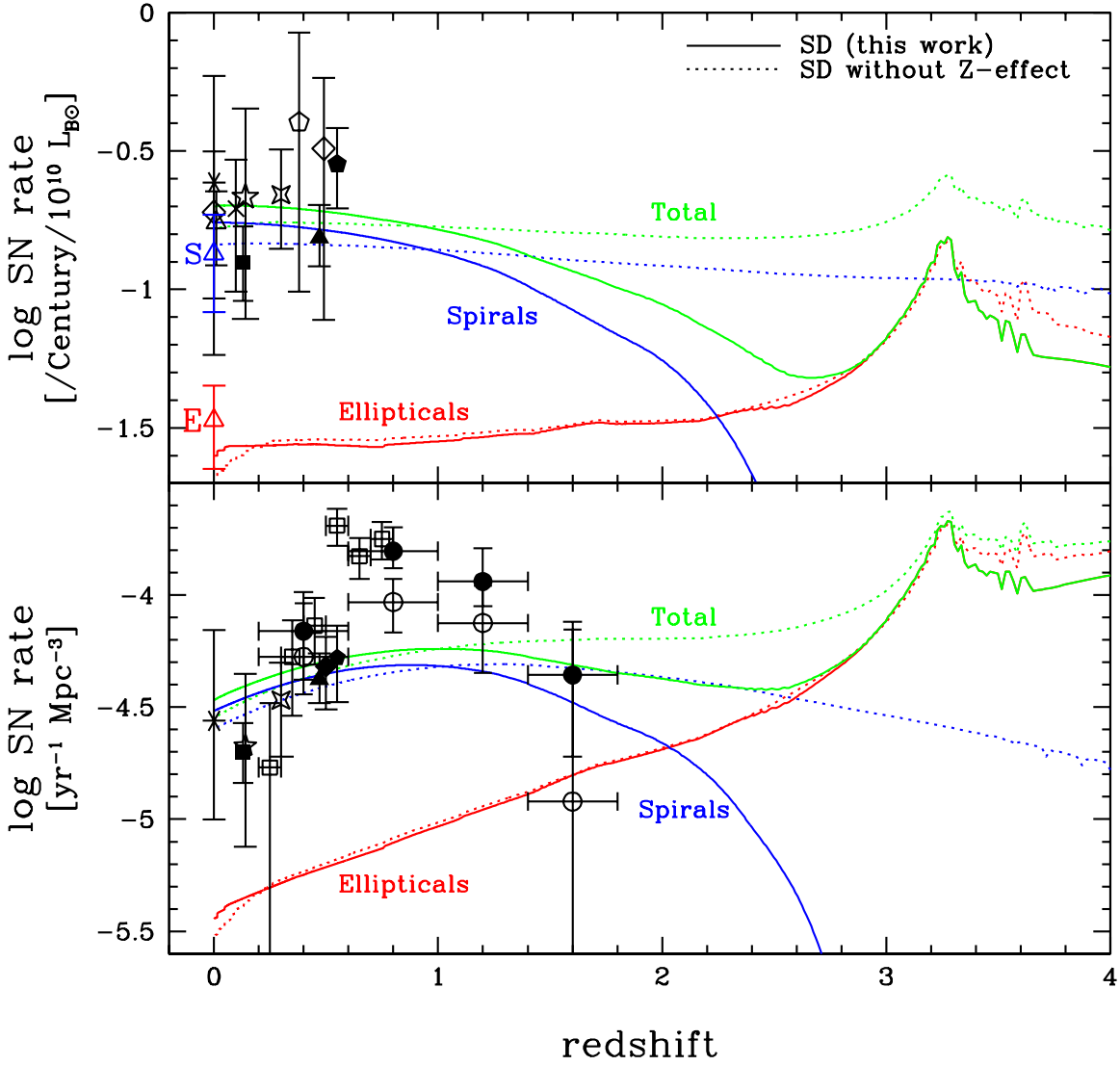


Fig. 13.— Same as Figure 11, but for our SD model with (solid lines) and without (dotted lines) metallicity effect.

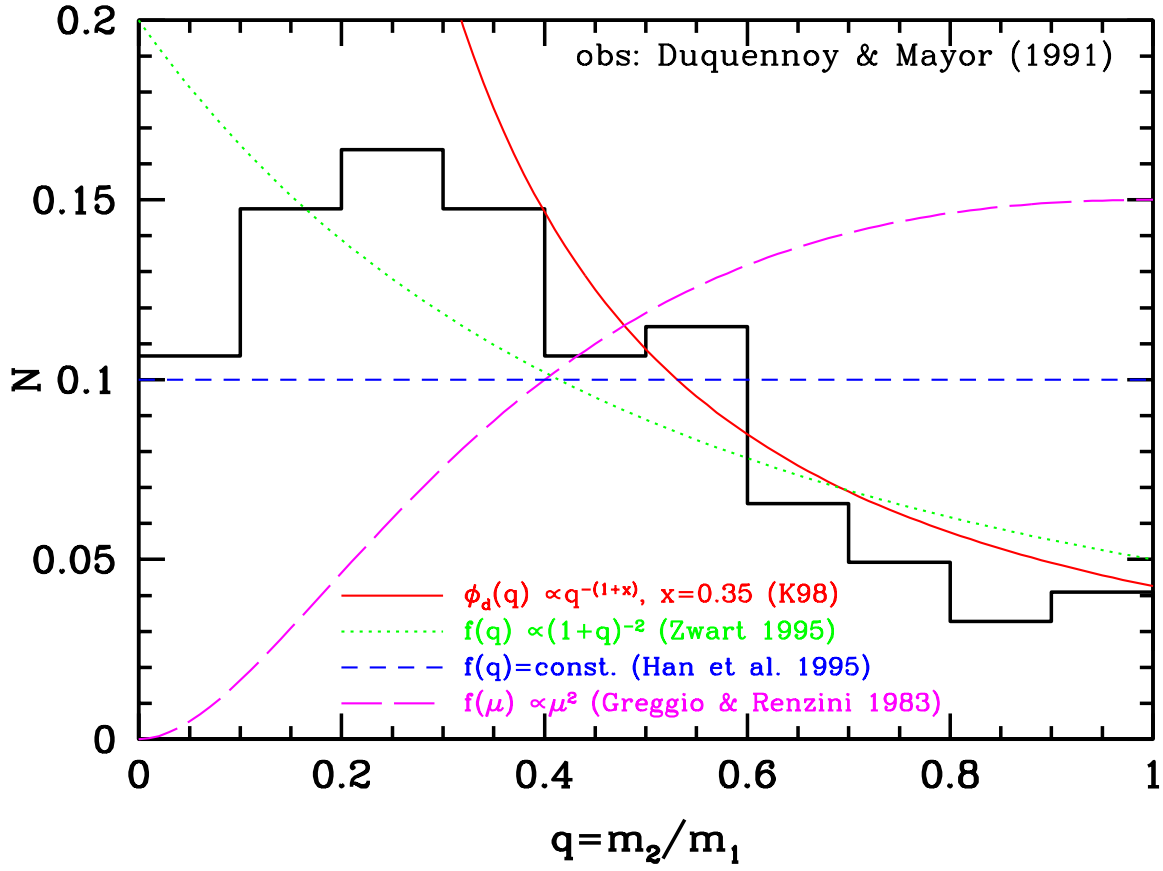


Fig. 14.— The distribution function of mass ratios; $\phi_d(m) \propto m^{-x}$ with $x = 0.35$ (solid line, K98), constant $f(\mu)$ (dotted line), constant $f(q)$ (short-dashed line), and $f(\mu) \propto \mu^\gamma$ with $\gamma = 2$ (long-dashed line, MR01). The histogram shows the observational data (Duquennoy & Mayor 1991).

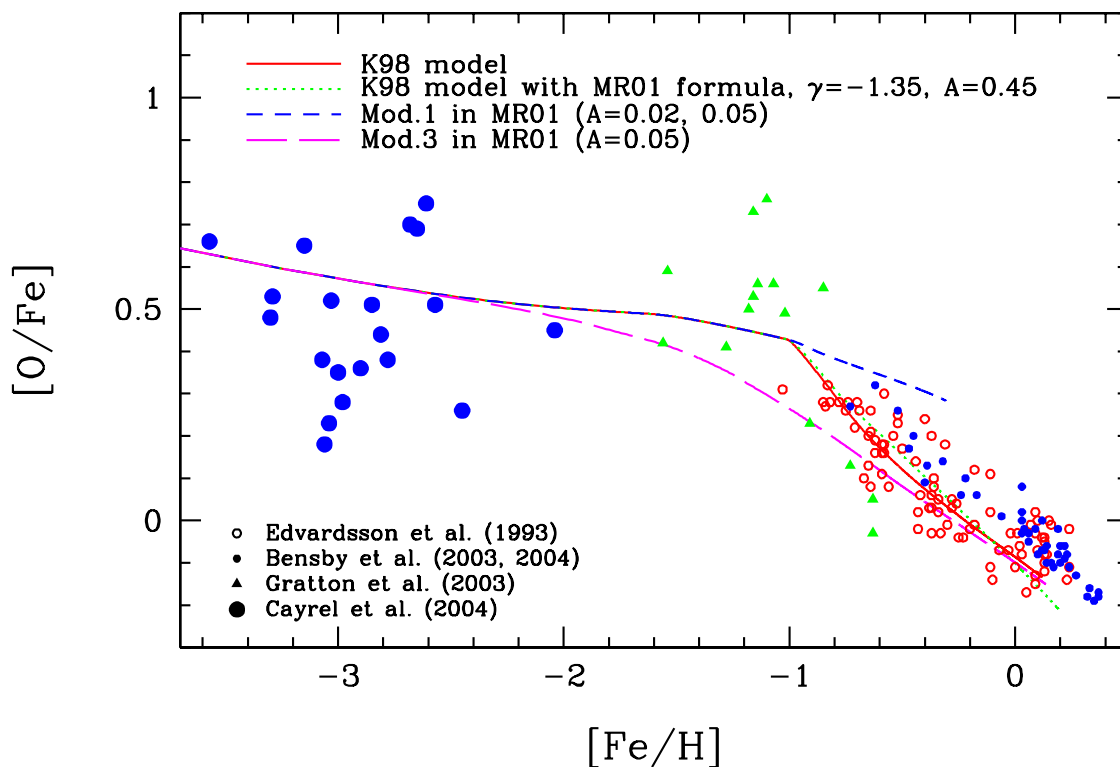


Fig. 15.— The $[O/Fe]$ - $[Fe/H]$ relation in the solar neighborhood for different SN Ia models. The solid line is for our original K98 model. The dotted line is calculated with MR01 formula Eq.[1] with K98 parameters. The dashed and long-dashed lines correspond to Model 1 and 3 in MR01, respectively. Observational data sources are: For disk stars, Edvardsson et al. (1993), small open circles; thin disk stars in Bensby et al. (2004), small filled circles; accretion component in Gratton et al. (2003), triangles. For halo stars, Cayrel et al. (2004), large filled circles.

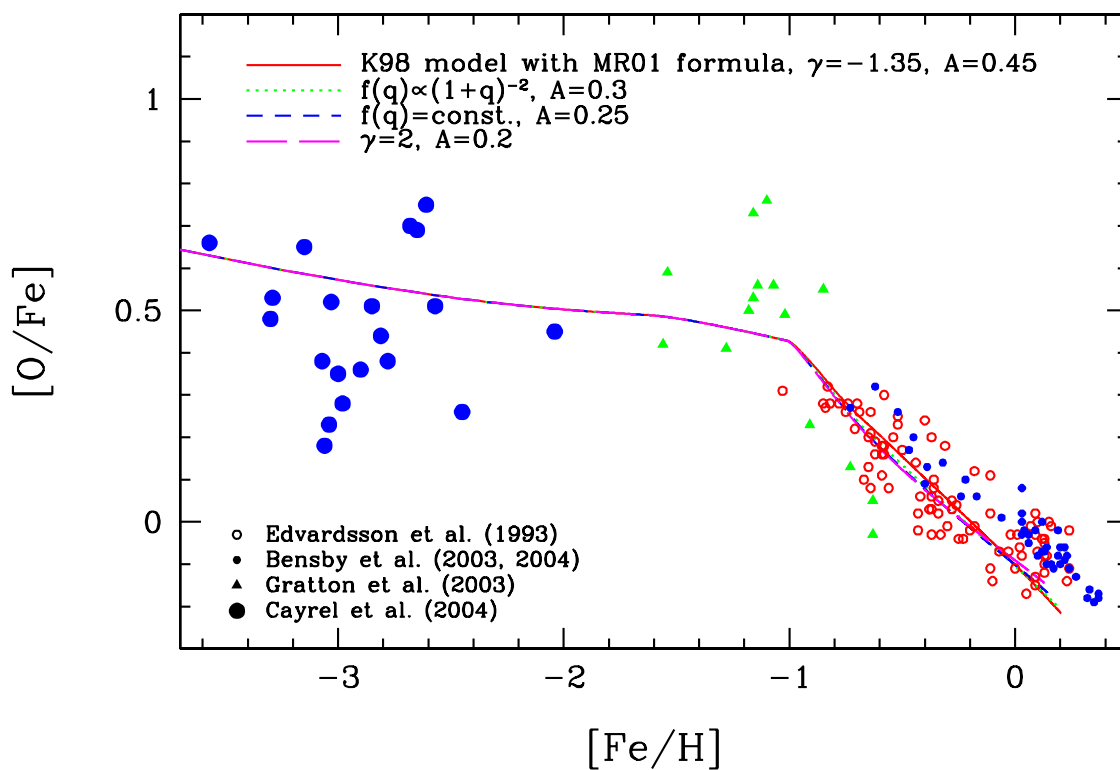


Fig. 16.— The same as Figure 15 but for different SN Ia models. The solid line is calculated with MR01 formula Eq.[1] with K98 parameters. The dotted and short-dashed lines are for the different functions of mass ratios, constant $f(\mu)$ and constant $f(q)$, respectively. The long-dashed line is for the same $f(\mu)$ as in MR01, but with our parameters of binary companions.

Table 6. Test results and predictions of the SN Ia models.

metallicity effect	SD		MR01	DD
	yes	no		
Lifetime [Gyr]	0.1 – 20		~ 0.3	~ 0.1
	peak at 0.1 & 1			
[α /Fe]-[Fe/H] relation	○	×	×	×
Present SN Ia rate in Es	○	○	○	×
Cosmic SN Ia rate history	peak at $z \sim 1$	constant	increase	increase
SNe Ia observed at $z \gtrsim 2$ in Ss?	few	yes	yes	yes

Table 2. The SN Ia rate of $1M_{\odot}$ simple stellar population in $[10^{-4} \text{ Gyr}^{-1}]$ as a function of time t_{Ia} [Gyr].

this work											
$Z = 0.002$			$Z = 0.004$			$Z = 0.02$			$Z = 0.05$		
t_{Ia}	$\mathcal{R}_{\text{Ia,t}}$	$\mathcal{R}_{\text{Ia,t}}$	t_{Ia}	$\mathcal{R}_{\text{Ia,t}}$	$\mathcal{R}_{\text{Ia,t}}$	t_{Ia}	$\mathcal{R}_{\text{Ia,t}}$	$\mathcal{R}_{\text{Ia,t}}$	t_{Ia}	$\mathcal{R}_{\text{Ia,t}}$	$\mathcal{R}_{\text{Ia,t}}$
	RG	MS		RG	MS		RG	MS		RG	MS
45.15	0	0	57.50	0	0	84.76	0	0	78.29	0	0
27.16	0	0	32.39	0	0	48.76	0	0	44.78	0	0
17.08	0	0	19.56	0	0	29.17	0	0	27.04	0.017	0
11.33	0.041	0	12.53	0.033	0	18.59	0.022	0	17.24	0.074	0
7.974	0.190	0	8.413	0.156	0	12.36	0.103	0	11.00	0.111	0
5.891	0.270	0	5.929	0.224	0	8.575	0.149	0	7.596	0.160	0
4.533	0.361	0	4.265	0.317	0	6.026	0.210	0	5.563	0.243	0
3.563	0.463	0	3.165	0.426	0	4.501	0.289	0	4.151	0.336	0
2.812	0.556	0	2.519	0.575	0	3.462	0.400	0	3.322	0.435	0
2.271	0.544	0	1.998	0.764	0	2.783	0.520	0	2.607	0.585	0
1.807	0	0	1.629	0.919	0	2.234	0.659	0	2.082	0.717	0
1.502	0	0	1.357	1.342	0	1.845	0.788	0	1.793	0.976	0
1.262	0	0.096	1.142	2.109	0.170	1.540	0.961	0.078	1.557	1.358	0.110
1.063	0	1.796	1.129	2.658	3.441	1.303	1.362	1.763	1.412	1.490	1.928
0.903	0	2.070	1.117	3.100	4.355	1.112	2.151	2.784	1.287	1.621	2.099
0.779	0	2.908	0.979	0	3.124	1.108	2.727	3.529	1.119	1.593	2.062
0.676	0	4.555	0.864	0	2.453	1.105	3.494	4.523	0.979	1.568	2.030
0.673	0	5.479	0.766	0	2.728	0.981	2.380	3.081	0.862	1.751	2.266
0.669	0	6.595	0.683	0	3.020	0.876	1.816	2.351	0.763	1.944	2.516
0.596	0	4.535	0.612	0	3.329	0.783	1.973	2.555	0.676	2.138	2.768
0.533	0	3.339	0.550	0	3.654	0.702	2.135	2.764	0.603	2.341	3.030
0.475	0	0	0.497	0	3.998	0.630	2.325	3.010	0.538	2.572	3.329
0.425	0	0	0.450	0	4.359	0.568	2.523	3.266	0.482	2.815	3.644
0.386	0	0	0.409	0	5.476	0.514	3.097	4.009	0.434	3.504	4.536
0.351	0	0	0.374	0	6.634	0.467	0.261	4.828	0.392	4.266	5.522
0.268	0	0	0.296	0	7.534	0.356	0	5.502	0.295	4.910	6.356
0.212	0	0	0.239	0	8.224	0.278	0	6.027	0.228	0	6.997
0.161	0	0	0.184	0	1.750	0.206	0	7.288	0.167	0	8.519
0.135	0	0	0.157	0	0	0.171	0	9.33	0.137	0	10.97
0.114	0	0	0.135	0	0	0.144	0	13.02	0.114	0	15.45
0.094	0	0	0.112	0	0	0.116	0	15.61	0.090	0	18.81
0.075	0	0	0.092	0	0	0.093	0	17.26	0.071	0	22.22
0.062	0	0	0.077	0	0	0.075	0	0	0.057	0	9.051
0.052	0	0	0.065	0	0	0.063	0	0	0.048	0	0
0.045	0	0	0.056	0	0	0.053	0	0	0.040	0	0

Table 2—Continued

this work											
$Z = 0.002$			$Z = 0.004$			$Z = 0.02$			$Z = 0.05$		
t_{Ia}	$\mathcal{R}_{\text{Ia},t}$	$\mathcal{R}_{\text{Ia},t}$	t_{Ia}	$\mathcal{R}_{\text{Ia},t}$	$\mathcal{R}_{\text{Ia},t}$	t_{Ia}	$\mathcal{R}_{\text{Ia},t}$	$\mathcal{R}_{\text{Ia},t}$	t_{Ia}	$\mathcal{R}_{\text{Ia},t}$	$\mathcal{R}_{\text{Ia},t}$
	RG	MS		RG	MS		RG	MS		RG	MS
0.039	0	0	0.050	0	0	0.046	0	0	0.035	0	0
0.034	0	0	0.044	0	0	0.041	0	0	0.030	0	0

Table 3. The SN Ia rate of $1M_{\odot}$ simple stellar population in [10^{-4} Gyr $^{-1}$] as a function of time t_{Ia} [Gyr].

K98						MR01	DD
$Z = 0.002$			$Z = 0.02$				
t_{Ia}	$\mathcal{R}_{\text{Ia},t}$	$\mathcal{R}_{\text{Ia},t}$	t_{Ia}	$\mathcal{R}_{\text{Ia},t}$	$\mathcal{R}_{\text{Ia},t}$	$\mathcal{R}_{\text{Ia},t}$	$\mathcal{R}_{\text{Ia},t}$
	RG	MS		RG	MS		
45.15	0	0	84.76	0	0	0.003	0
27.16	0	0	48.76	0	0	0.007	0
17.08	0	0	29.17	0	0	0.017	0
11.33	0.053	0	18.59	0.028	0	0.039	0.006
7.974	0.246	0	12.36	0.134	0	0.080	0.017
5.891	0.350	0	8.575	0.193	0	0.156	0.039
4.533	0.468	0	6.026	0.272	0	0.284	0.087
3.563	0.599	0	4.501	0.375	0	0.535	0.168
2.812	0.720	0	3.462	0.518	0	0.913	0.302
2.271	0.705	0	2.783	0.547	0	1.463	0.449
1.807	0	0	2.234	0	0	1.668	0.624
1.502	0	0	1.845	0	0	1.945	0.832
1.262	0	0.335	1.540	0	0.269	2.165	1.090
1.063	0	6.234	1.303	0	6.117	2.397	1.402
0.903	0	7.186	1.112	0	9.664	4.652	1.779
0.779	0	10.10	1.108	0	12.25	127.1	1.787
0.676	0	15.81	1.105	0	15.70	5.624	1.794
0.673	0	19.02	0.981	0	10.69	2.780	2.144
0.669	0	22.89	0.876	0	8.160	2.875	2.543
0.596	0	15.74	0.783	0	8.867	2.963	3.012
0.533	0	11.59	0.702	0	9.187	3.057	3.543
0.475	0	0	0.630	0	0	3.143	4.165
0.425	0	0	0.568	0	0	3.285	4.868
0.386	0	0	0.514	0	0	3.425	5.657
0.351	0	0	0.467	0	0	4.014	6.542
0.268	0	0	0.356	0	0	3.873	9.824
0.212	0	0	0.278	0	0	4.427	14.24
0.161	0	0	0.206	0	0	4.510	22.33
0.135	0	0	0.171	0	0	5.267	25.27
0.114	0	0	0.144	0	0	5.522	27.56
0.094	0	0	0.116	0	0	5.598	12.86
0.075	0	0	0.093	0	0	5.274	1.004
0.062	0	0	0.075	0	0	4.807	0.086
0.052	0	0	0.063	0	0	4.066	0
0.045	0	0	0.053	0	0	2.949	0

Table 3—Continued

K98						MR01	DD
$Z = 0.002$			$Z = 0.02$				
t_{Ia}	$\mathcal{R}_{\text{Ia,t}}$	$\mathcal{R}_{\text{Ia,t}}$	t_{Ia}	$\mathcal{R}_{\text{Ia,t}}$	$\mathcal{R}_{\text{Ia,t}}$	$\mathcal{R}_{\text{Ia,t}}$	$\mathcal{R}_{\text{Ia,t}}$
	RG	MS		RG	MS		
0.039	0	0	0.046	0	0	1.532	0
0.034	0	0	0.041	0	0	0	0